DSPACE

https://dspace.org/

Mapping and monitoring the Seriphium plumosum encroachment in the rangelands of KwaZulu-Natal using landsat earth observation data

Shangase, Cyprian Bhekinkosi

2025
University of the Witwatersrand, Johannesburg
https://hdl.handle.net/10539/50260
Shangase, Cyprian Bhekinkosi. (2025). Mapping and monitoring the Seriphium plumosum encroachment in the rangelands of KwaZulu-Natal using landsat earth observation data [Master's dissertation, University of the Witwatersrand, Johannesburg]. WIReDSpace. https://hdl.handle.net/10539/50260

Downloaded from a DSpace repository. https://dspace.org/

Mapping and monitoring the *Seriphium plumosum* encroachment in the rangelands of KwaZulu-Natal using landsat earth observation data

Student: Cyprian Bhekinkosi Shangase (1502061)

A research report submitted, in partial fulfilment of the requirements for the degree of Master of Science in Geographical Information Systems and Remote Sensing, to the School of Geography, Archaeology & Environmental Studies, in the Faculty of Science at the University of the Witwatersrand, Johannesburg, South Africa

Supervisor: Prof Cletah Shoko

School of Geography, Archaeology and Environmental Studies

Co-Supervisor: Dr Jolene Fisher

School of Animal, Plant and Environmental Science

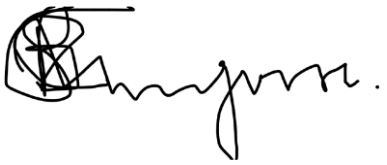
DECEMBER 2025

PLAGIARISM DECLARATION

I declare that this Research Report is my own, unaided work. This Research Report is being submitted for the Degree of Master of Science in Geographical Information Systems and Remote Sensing at the University of the Witwatersrand, Johannesburg. It has not been submitted before for any examination or degree at any other University.

Student Name: Cyprian Bhekinkosi Shangase

Student Number: 1502061

Signature: 

Date: 11 DECEMBER 2025

AI DECLARATION

Wits University Faculty of Science post-graduate student AI declaration

I understand that the use of generative AI tools (such as ChatGPT or similar) without explicitly declaring such use constitutes a form of plagiarism and is classified by Wits University as academic misconduct.

I declare that in the course of conducting the research towards my degree or in the preparation of this thesis/dissertation/research report (select one by marking with an X):

I **did not** make use of generative AI tools ☐

I **did** make use of generative AI tools for the following (tick all that apply):

1. Idea Generation (research problem/design, hypothesis) ☐
2. Sourcing Related Work (summarising, identifying sources) ☐
3. Methods and Experiment Design (experiment setup, model tuning) ☐
4. Data Analysis (presentation, coding, interpretation) ☐
5. Theoretical Development (theorem proving, conceptual analysis) ☐
6. Code Development (generating algorithms, writing scripts) ☒
7. Presentation (rendering graphics, formatting) ☐
8. Editing (grammar, readability) ☒
9. Writing (text generation, document structuring) ☐
10. Citation Formatting (structuring, organising) ☒

If other uses were involved, please specify below:

Generative AI tool used (list all)	**Used for?**
Grammarly	Grammer Editing and Readability
Google Colab and Google Earth Engine	Code Development and Algorithms
MyBib	Citation Formating (structuring, organising)

If generative AI tools were used as an integral part of the experimental design or in the direct execution of my research, I confirm that details of this use are clearly outlined in the relevant experimental/methodology chapters of my thesis/dissertation/research report.

Student number:

1502061

Candidate signature:



Date: 11 DECEMBER 2025

DEDICATION

I dedicate this work to my wife and kids for their encouragement and unwavering support throughout the years on this journey. I am forever grateful.

ACKNOWLEDGEMENTS

I acknowledge and express my gratitude to my supervisors, Prof Cletah Shoko and Dr Jolene Fisher, for their professional and invaluable guidance throughout this process. My fellow students at Wits are also acknowledged for encouragement, support, and assistance with data modelling and analysis. Special thanks to my employer for affording me the time to conduct my research and a bursary towards my studies. I could not have asked for a better employer.

ABSTRACT

Environmental and climate change are the significant drivers of rangeland degradation. This study monitored and mapped the historical and present, as well as modelled the future encroachment of *Seriphium plumosum* L (Asteraceae) in the rangeland of Nquthu Municipality area, KwaZulu-Natal Province, South Africa using Landsat-8 OLI time series images and Maximum Entropy (MaxEnt) model. High accuracy indicators were achieved, with overall accuracy (OA) of 90.1% and a Kappa of 0.84 for 2014 image, and an OA of 93.5% and a Kappa of 0.87 for 2024 image, with Area Under Curve values above 0.90. Temperature and precipitation-based variables were the main drivers of *S. plumosum* encroachment. Suitable habitat for *S. plumosum* is predicted to increase from 23.6% to approximately 32.4% by year 2040 and will encroachment to more gentle slopes while steeper slopes will be unsuitable and will challenge a sustainable and more adaptive rangeland management approach by land manages.

Keywords: Bio-climatic data, GEE, Landsat, LULC, MaxEnt Model, Random Forest, Rangeland, *S.plumosum*

TABLE OF CONTENTS

PLAGIARISM DECLARATION ..... **I**

AI DECLARATION ..... **II**

DEDICATION ..... **III**

ACKNOWLEDGEMENTS ..... **IV**

ABSTRACT ..... **V**

LIST OF FIGURES ..... **VIII**

LIST OF TABLES ..... **IX**

LIST OF ABBREVIATIONS ..... **X**

CHAPTER ONE: GENERAL INTRODUCTION **1**

1.1. Introduction 1

1.2. Background 1

1.3. Problem Statement 3

1.4. Research Aims and objectives 3

1.5. Structure of the research report 4

CHAPTER TWO: LITERATURE REVIEW **5**

2.1. Introduction 5

2.2. Ecology and management of *Seriphium plumosum* 5

2.3. Monitoring and control of *Seriphium plumosum* encroachment in rangelands 7

2.4. Multispectral remote sensing of invasive plant species 8

2.5. Hyperspectral remote sensing of invasive plant species 10

2.6. Spectral characteristics of invasive plant species 11

2.7. Machine learning algorithms used to discriminate invasive plant species 13

2.8. The use of species distribution models in invasive plant species ecology 14

2.9. Cloud computing platforms used in the remote sensing of invasive plant species 15

2.10 Conclusion 16

CHAPTER THREE: MATERIALS AND METHODS **18**

3.1. Introduction 18

3.2. Study Area 18

3.3. Collection of field reference data 19
3.4. Image data collection 22
3.5. Image classification using Random Forest 23
3.6. Classification accuracy assessment 23
3.7. Extraction of spectral indices 24
3.8. Implementation of SHaply Additive exPlanations. 25
3.9. Application of the Species Distribution Model 25
3.9.1. Bioclimatic data acquisition and processing 25
3.9.2. Maximum Entropy model implementation and performance validation procedure 27

CHAPTER FOUR: RESULTS 30

4.1. Introduction 30
4.2. Image classification accuracy assessment 30
4.3. Land use and land cover change detection 32
4.4. Measurement of Random Forest model variable feature importance 35
4.5. Maximum Entropy model performance validation 37
4.5.1. Accuracy assessment 37
4.5.2. Importance of climatic variables and model preferences 39
4.6. Contribution and response of predictor variables 40
4.7. Current and future habitat suitability modelling for *Seriphium plumosum* 41

CHAPTER FIVE: DISCUSSION 43

5.1. Introduction 43
5.2. Random Forest image classification and variable importance 43
5.3. Spatial variations in Land Use and Land Cover change. 45
5.4. Bio-climatic variable contribution to model prediction 46
5.5. Recommendations and limitations 48
5.6. Conclusion 48

LIST OF REFERENCES 50

LIST OF FIGURES

Figure 1: *Seriphium plumosum* in different penological stages: A) flowering stage with bright purple to white flowers, B) dense mature shrubland, and C) young fresh seedling stage. (Source: Author). 6

Figure 2: Spectral reflectance of *Seriphium plumosum* in comparison to grass (Adopted from Dubula et al,.2016) 12

Figure 3: Locality map of the study area within Nquthu Local Municipality in KwaZulu-Natal Province, South Africa. 19

Figure 4: Methodology workflow conceptual chart. 29

Figure 5: RF classified image: A) for 2014 and B) for 2024 showing land use and land cover (LULC) in the study area located in the Nquthu Municipal area, KwaZulu-Natal, South Africa 33

Figure 6: Land Use and Land Cover (LULC) change (%) for different classes in the study area located in the Nquthu Municipal area, KwaZulu-Natal, South Africa. 34

Figure 7: Calculated changes per class LULC class showing class increases and decreases in the study area located in the Nquthu Municipal area, KwaZulu-Natal, South Africa. 34

Figure 8: A) mean SHAP values for the 2014 RF model and B) is for the 2024 RF model. 36

Figure 9: MaxEnt model A) Sensitivity vs Specificity and B) Omission and predicted area for *Seriphium plumosum* prediction. 38

Figure 10: Distribution accuracy of *Seriphium plumosum* species true presence prediction at 0.5 cutoff. 38

Figure 11: AUC of variables and their importance. 39

Figure 12: Variable response curves for the top two contributors (TPI and Bio-2) and bottom two contributors (Bio-14 and Bio-19) affecting *Seriphium plumosum* distribution. 40

Figure 13: *Seriphium plumosum* habitat suitability maps showing A) current and B) predicted future distribution in the study area located in the Nquthu Municipal area, KwaZulu-Natal, South Africa 42

LIST OF TABLES

Table 1: Summary and general description of the standard land cover classes used in the study, source: South African National Land Cover (SANLC 2016). 20

Table 2: Training and validation samples for each 2014 image data. 21

Table 3: Training and validation samples for each 2024 image data. 21

Table 4: Landsat 8-OLI spatial and spectral characteristics and their resolutions. Source: NASA Landsat Science (2025). 22

Table 5: Indices selected to supplement raw spectral image bands for classification. 24

Table 6: Description of bioclimatic variables used for MaxEnt model prediction sourced from Fick et al., (2017). 26

Table 7: Confusion matrix for A) 2014 and B) 2024 accuracy assessment of LULC. 31

LIST OF ABBREVIATIONS

ANN	Artificial Neural Networks
BSI	Bare Soil Index
CART	Classification and Regression Trees
Colab	Google Colaboratory
ESRI	Environmental Systems Research Institute
FAO	Food and Agriculture Organisation
GIS	Geographic Information Systems
GPS	Global Positioning System
GEE	Google Earth Engine
GEEP	Google Earth Engine Pro
IPSs	Invasive Plant Species
LULC	Land Use and Land Cover
MaxEnt	Maximum Entropy
NDVI	Normalised Difference Vegetation Index
NDWI	Normalised Difference Water Index
RF	Random Forest
RS	Remote Sensing
SAVI	Soil Adjusted Vegetation Index
SDM	Species Distribution Model
SHAP	SHapley Additive exPlanations
SVM	Support Vector Machines
SPOT	Satellite Probatoire d'Observation de la Terre
TPI	Topographic Position Index
UAVs	Unmanned Aerial Vehicles

CHAPTER ONE: GENERAL INTRODUCTION

1.1. Introduction

This chapter introduces the study by offering a brief overview of rangelands, highlighting their importance in commercial agriculture, and outlining the current global and local threats they face. The utilisation of various remote sensing technologies to monitor these threats will also be examined. Lastly, this chapter will clarify the problem statement by explaining the reasons for the research and specifying the aims and questions it will address.

1.2. Background

Rangelands cover almost half of the Earth's land surface and support around three-quarters of the world's population (Feng & Fu, 2013). Significant drivers of rangeland conversion include environmental and climate change, and habitat fragmentation. According to the Food and Agriculture Organisation (FAO) (2011), many countries in sub-Saharan Africa encounter unique challenges due to global climate change. These challenges necessitate initiatives that aim to boost agricultural productivity while strictly adhering to land-use change management principles and policies to mitigate environmental degradation (Mussa et al., 2016b). Given the ongoing decline in global biodiversity, it is crucial to monitor grassland biomes, particularly for conservation efforts. McCord et al. (2022b) noted that land managers require reliable information to understand the current state and condition of rangeland resources. Rangeland ecosystems support a diverse array of plant and animal species by providing habitat and grazing for herbivores. According to the FAO and the World Bank (2008), rangelands provide 10% of the global meat supply and support an estimated 200 million pastoralists and their herds of cattle, small ruminants, and other ungulates. Grazing livestock on rangelands provides a vital source of meat, milk, and other animal products (Reynolds et al., 2007). Rangelands also serve as a vital economic resource for pastoral communities worldwide. According to Jama and Zeila (2005), the deterioration in environmental quality and rangeland productivity is attributed to a combination of human and climatic factors.

Rangeland degradation constitutes a worldwide phenomenon that poses a direct threat to global food security (FAO, 2008). Poor and inappropriate land-use management practices contribute to land degradation in semi-arid regions, particularly in crucial savanna rangelands across various African countries (Maphanga et al., 2022). However, the level of degradation in developing countries is difficult to measure due to insufficient monitoring and a lack of data availability. For example, in Ethiopia, a common form of rangeland degradation results from the encroachment of rangelands by both native and alien plant species (Angassa & Oba, 2008; Gemedo et al., 2006). According to Ramoelo et al. (2018), bush encroachment decreases grazing capacity and ecosystem function, leading to a decline in Gross Domestic Product (GDP) of 10-17% globally. In southern Africa, invasive bush species are encroaching on savanna and grassland rangelands. This phenomenon has adverse effects and implications on economic viability, particularly in terms of reduced agricultural productivity and output (Musa et al., 2016). Archer et al. (2001) reported that bush encroachment of woody vegetation into grasslands has been a significant problem for the ranching and agricultural industries worldwide, directly affecting livestock productivity. Maphanga (2022) states that climatic variability worsens the devastating effects of bush encroachment on both the sociology and ecology of a region. In South Africa, the increase in bush encroachment and overgrazing are the significant factors driving land degradation in rangelands. The impacts of such encroachment by the observed species depend on the functional traits of the species involved and the level or stage of encroachment (Eldridge & Ding, 2021).

The utilisation of remote sensing technologies, in conjunction with statistical modelling tools and machine learning algorithms, presents an opportunity to examine rangeland invasion across various temporal and spatial contexts, as data can be cost-effectively captured and analysed (Landgrebe, 1999). Remote sensing data are now readily available, for example, SPOT, Landsat and Sentinel image data and are cost-effective tools for mapping and monitoring extensive areas (Freeman et al., 2002). Historically, land cover change mapping was conducted using manual interpretation and digitisation of aerial photographs, which proved to be a time-consuming exercise (Everitt & Deloah, 1990). With the recent advancement in multispectral and hyperspectral satellite data, automated classification methods such as maximum likelihood and unsupervised clustering techniques are now widely employed (Sawaya et al., 2003).

1.3. Problem Statement

Seriphium plumosum (Bankrupt bush) is native to South Africa, and numerous studies have demonstrated that it is a dominant species in most South African grassland biomes, including those in the provinces of KwaZulu-Natal, Free State, Mpumalanga, Eastern Cape, and Gauteng (Morgenthal, 2018 and Ruthford et al., 2006). The rate of its encroachment has recently increased in semi-arid grassland regions due to changes in environmental and ecological conditions that favour its invasion (Snyman, 2012a). It reduces the production potential of rangelands by up to 65% when encroachment reaches a density of 2000 shrubs per hectare (Snyman, 2012a). This results in a decrease in the availability of edible vegetation for grazing livestock, such as sheep, goats, and cattle (Snyman, 2012b). This phenomenon is also associated with considerable economic loss when eradication and control methods are implemented (Mtyobila & Shoko, 2024).

In the province of KwaZulu-Natal, no studies have employed a combination of remote sensing techniques and species distribution modelling (SDM) methods to discriminate *S. plumosum* as a target species from other bush encroachers or grass species, to compare its spread across different land cover types, or to model its potential future distribution. To address this gap, this study examines the spatial and temporal characteristics of rangeland invasion in three scenarios: historical, present, and future, in an active agricultural rangeland that remains poorly understood.

1.4. Research Aims and objectives.

This study aims to monitor and map the spatial and temporal distribution of *Seriphium plumosum* over a 10-year period (from 2014 to 2024) in the rangeland of Nquthu Municipal area, KwaZulu-Natal Province, South Africa

The following are the research questions;

- Can Landsat-8 image data combined with the Random Forest (RF) algorithm successfully detect and delineate the distribution of *S. plumosum* in rangelands?
- What is the amount of encroachment and the spatial distribution of *S. plumosum* over 10 years (2014 to 2024)?
- Which environmental variable (s) are the most influential and responsible for the *S. plumosum* invasion?

- Which areas are most vulnerable to invasion by *S. plumosum* in the study area?

The following are research objectives;

- To evaluate the functional performance of the Random Forest as a non-parametric classifier in combination with Landsat-8 image data to discriminate *S. plumosum* in a heterogeneous landscape
- To map the historical and current encroachment of *S. plumosum* using Landsat-8 imagery in Google Earth Engine over ten years
- To model the current and future habitat suitability of the *S. plumosum* for the purposes of identifying areas that are vulnerable to future encroachment using the Maximum Entropy
- To identify the most influential bio-climatic variables responsible for its distribution in the rangeland

1.5. Structure of the research report

This research report is divided into four different chapters. Chapter one introduces the topic by providing a brief background on rangelands, their management, and the threats they face. The chapter concludes by presenting a brief research problem statement, along with its aims and questions that will be addressed. Chapter two reviews the literature and examines topics directly related to this research. Historical and recent studies that have contributed to the encroachment of rangelands, the ecology of *S. plumosum*, and the remote sensing and geostatistical modelling literature will be discussed. The third chapter outlines the methods that will be employed to answer the study's key questions and fulfil its aims and objectives. Furthermore, it describes the sampling area (study area), the sampling design, the data collection procedure, the data preparation procedure, and the statistical analysis. The fourth chapter systematically presents the results from the methods described in the third chapter. Chapter Five presents a comprehensive and concise discussion of the implications of the problem the study addresses, concluding with a discussion of its limitations and a proposal for further research directions and recommendations.

CHAPTER TWO: LITERATURE REVIEW

2.1. Introduction

The evolution of multispectral and hyperspectral sensors has proven to be a cost-effective, reliable, and valuable tool for mapping, classifying, and predicting land invasion by native and non-native plant species. This chapter reviews the literature associated with key subject matters, namely, the remote sensing of invasive plant species (using multi-spectral and hyperspectral systems), machine learning algorithms such as random forest (RF) and support vector machines (SVMs), and management and control strategies for encroachment by *S. plumosum.* Lastly, the use of predictor models for species distribution, such as the MaxEnt model, which is widely used in ecological studies, will also be interrogated.

*2.2.*Ecology and management of *Seriphium plumosum*

Seriphum plumosum, commonly known as Bankrupt bush or Slangbos, is an indigenous, woody, dwarf shrub that encroaches into grasslands and some savannah biomes (Snyman, 2012). It is a woody, dwarf shrub that can reach a crown of 1 m^2 and a height of up to 1 m, making it very successful at dominating grassland areas where its extensive root system outcompetes grass species for water and nutrients (Snyman, 2012). It produces thousands of seeds per year, which are easily dispersed by various agents, such as wind and animals, over large distances (Snyman, 2010). Due to its large crown (1 m^2), grass species are easily displaced (Brewer, 2002). Its small, light green leaves make it adaptable to surviving for a long time in drier conditions, and its seeds can remain dormant and buried in the soil for up to five years until conditions are favourable for germination, and are highly stimulated by veld fires (Snyman, 2012a). Figure 1 shows *S. plumoum* at different stages of its life cycle. It has aromatic but volatile oils that produce an unpleasant smell, making it unpalatable to browsing or grazing animals (Jordaan, 2009). In South Africa, the flowering season of the shrub is well defined, extending from autumn/winter (April to June) into spring, with a noticeable peak from September to November (Mokaka et al. 2016). Snyman (2012b) discovered that *S. plumosum* dominates sandier soils with low pH and favours soils with up to 24% clay content, which become encroached if well drained, and thrives on disturbed or rocky surfaces (Snyman, 2012a). The amount of annual rainfall sufficient for the invasion of *S. plumosum* ranges from 620 to 750 mm per year in semi-arid and mesic biomes (Wepener, 2007). *S. plumosum* encroachment suppresses herbaceous species, leading to biodiversity loss, reduced grazing

capacity and degradation of the natural resources. *S. plumosum* is listed as a proclaimed encroacher plant under regulation 16 of the Conservation of Agricultural Resources Act 43 (CARA) due to its capacity to reduce grazing land (Moore & Van Niekerk, 1987). According to Avenant (2015), its distribution in South African rangelands is estimated to be around 50,000 hectares, which mostly dominates semi-arid grassland biomes of the Mpumalanga, Free State, Northwest and Eastern Cape provinces (Snyman, 2011). The encroachment is also reported in other countries outside South Africa, such as Angola, Mozambique, and Zimbabwe (Koekemoer, 2001), as well as in Madagascar and the USA (Schmidt et al., 2002). Its spread in many regions is exacerbated by, among other things, changes in environmental and/or ecological conditions (Snyman, 2012b).

According to Badernhorst et al. (2009), it is common that woody plant species vary seasonally in response to biotic and abiotic factors, and their germination is influenced by fire. After a fire event, the nutrient concentration rises, particularly in the first growing season, as noted by Snyman (2010). General land use changes, such as the transition from sheep to cattle farming, are suspected of influencing the rapid encroachment rate of *S. plumosum* (Snyman, 2010). This land-use switching of grazing preference in angulates is observed, where sheep utilise younger plants and only browse the seed tops, which may control the spatial distribution of *S. plumosum* (Snyman, 2010). Although there is a common perception that the plant is largely unpalatable, reports from farmers indicate that Merino and Dorper sheep do feed on the encroacher *S. plumosum* at an early and seedling stage. In contrast, cattle are reported to avoid the plant entirely.



Figure 1: *Seriphium plumosum* in different penological stages: A) flowering stage with bright purple to white flowers, B) dense mature shrubland, and C) young fresh seedling stage. (Source: Author).

2.3. Monitoring and control of *Seriphium plumosum* encroachment in rangelands

Monitoring invasive plant species (IPSs) has evolved over the years, shifting from traditional methods, such as field surveys, to advanced remote sensing platforms (Munyati et al., 2009). These methods were time-consuming and proved to have various limitations. Dube et al. (2020) highlight that remote sensing techniques utilising multispectral and hyperspectral data have produced essential results to date. Recently, the use of remote sensing platforms to map, quantify, and monitor invasive alien plant species distribution has advanced, offering new opportunities for critical information necessary for managing and monitoring IPSs (Ludwig et al., 2016; Worku, 2018). For example, the advancement of hyper and multispectral remote sensing sensors, including Landsat, Satellite Pour L'Observation de la Terre (SPOT), Sentinel-1 and 2, and Unmanned Aerial Vehicles (UAVs), among others (Lass et al., 2005), has delivered essential and cost-effective technologies for monitoring the spatial and temporal distribution of both invasive (native and non-native) plant species. While advancements in various technologies and methods for controlling and managing invasive plant species are acknowledged, early detection remains paramount.

The control of *S. plumosum* encroachment in rangelands is primarily achieved through chemical and mechanical methods (Jordaan, 2009 and Snyman, 2012b). Chemical control involves the use of chemicals such as herbicides. This presents challenges, as certain chemicals can harm the natural environment, even though it may be the most cost-effective way to manage *S. plumosum.* Mechanical control refers to the removal of *S. plumosum* through manual methods or machinery tools. Both methods present challenges, such as limited access due to terrain or topography (Jordaan, 2009), and some infestations may be unreachable. Mechanical control is labour-intensive and costly over large areas. This method has also been shown to be ineffective when the stem is not correctly cut below the soil surface, leading to coppicing of the plant (Snyman, 2010a). Currently, there are no known biological methods to control the invasion of rangelands by *S. plumosum*, highlighting an existing gap in the literature. The limited amount of information in the literature necessitates an urgent need to develop or enhance mapping methods of its spatial and temporal distribution to improve control mechanisms for its invasion. Moreover, the effects of its invasion on agricultural rangelands and ecological systems underscore the necessity to establish its geographical extent for urgent mitigation strategies.

2.4. Multispectral remote sensing of invasive plant species

Multispectral imagery is more cost-effective than conventional methods and gathers data across three to six spectral bands (Peerbhay et al., 2016). The availability of moderate spectral image data in South Africa has been made possible through an agreement between the South African National Space Agency (SANSA) and Airbus Defence and Space (ADS), for example, to ensure an uninterrupted supply of SPOT imagery (Oumar, 2016). The benefit of this agreement is the availability of extensive archived data with enhanced spatial properties (Oumar, 2016). This agreement has facilitated numerous studies on invasive ecology and the impact of native and non-native plant species in natural environmental ecosystems, for example, *P. hysterophorus* (Nigatu et al.,2010), Bracken fern: *Pteridium aquilinum* (Ngubane et al., 2014), Bugweed: *Solanum mauritianum* (Peerbhay et al., 2015), Bankrupt bush: *S. plumosum* (Dabula et al., 2016), Common lantana: *Lantana Camara* (Oumar, 2017), Parthenium: *P hysterophorus* (Roymani et al., 2017), *Acacia spp* (Masemola et al., 2020), Bankrupt bush: *S. plumosum* (Urban et al., 2021). Recent advancements in multispectral remote sensing technologies, including Landsat-9, Worldview, and Sentinel-2, mark a significant milestone in enhancing the quality of analysis required for mapping, quantifying, and performing predictive assessments of invasive species. Such enhancement includes the addition of the red edge band for enhanced mapping and detection of invasive species onboard the Sentinel-2 and Worldview-2/3. Landsat-9 also improved radiometric performance and calibration, although bands remained the same as Landsat-8. For instance, Ndlovu & Shoko (2023) and Mtyobila & Shoko (2024) employed Sentinel-2 to map and model Lantana camara accurately, achieving accuracy indicators ranging from 80% to 91% for both user and producer accuracies. Additionally, Forsyth et al. (2014) utilised SPOT-6 imagery to map Pinus spp. with a convincing overall accuracy of 84%. Ngubane et al. (2014) compared the high-resolution World View-2 to SPOT-5 for bracken fern detection, achieving an overall accuracy of 72.22% with SPOT-5 and 91.67% with World View-2. Dubula et al. (2016) compared the performance of SPOT 5 and Landsat images in discriminating *S. plumosum* from grass species. However, they did not reach conclusive findings due to differences in species phenology, varying spectral measurements, weather conditions, and the temporal resolution of the images. Furthermore, spectral measurements were not taken in an ideal scenario, for example, sunny conditions which significantly influenced results. These were significant shortcomings of their study, and a proposal to upscale the same study to airborne and spaceborne remote sensing was made. Lastly, Urban et al. (2021) utilised Sentinel-1 and Sentinel-2 time series methods to delineate the distribution of *S.*

plumosum within the Free State Province of South Africa. The study combined the supervised random forest classifier and the Soil Adjusted Vegetation Index (SAVI) to predict the spread, achieving a precision accuracy of 80%.

Landsat-8 multispectral imagery was launched in 2013 as part of the Landsat programme and provides high-resolution imagery (Roy et al., 2014). Its main aim is to provide essential information on plant reflectance in visible, near-infrared (NIR), and shortwave infrared (SWIR) regions, which are sensitive to vegetation health (Retkute et al., 2025). Studies have demonstrated its success in various vegetation change detection and disease monitoring applications for plants (Retkute et al., 2025). Recently, Mogonong et al. (2024) used Landsat time series images (Landsat-5 TM, 7 ETM+ and 8-OLI) in combination with climate data to determine the influence of climate variability on LULC in three different rural municipalities of South Africa over a 38-year period, through the use of time series approach, and achieved above 80% overall accuracy of above 80%. Bhungeni et al. (2024) used Landsat-8 to evaluate the potential of different machine learning algorithms to map LULC in the uMngeni catchment in the Province of KwaZulu-Natal in South Africa. In this study, all machine learning algorithms, including Random Forest (RF), Support Vector Machine (SVM), Artificial Neural Networks (ANN), and Naïve Bayes (NB), achieved an overall classification accuracy of more than 80%, which is indicative of Landsat's influential spectral bands in classifying different classes. Landsat-9 was launched in 2021, which was an improvement of Landsat-8 spectral and spatial characterisation (Masek et al., 2020). Primarily, these changes improved the signal-to-noise ratio for targets such as dark features like forests and water bodies thus avoiding saturation in very dark or brighter objects (Masek et al.,2020; Xu et al., 2024), with a higher radiometric resolution of 14 bits from Landsat-8's 12 bits which is a significant improvement allowing a broader dynamic range in each spectral band (Gross et al.,2022). The success of multispectral sensors primarily stems from the strategic positioning of bands, which significantly improves the detection and discrimination of various vegetation types (Royimani et al., 2018). Despite the introduction of improved Landsat-9 multispectral data in 2021, this study utilised Landsat-8 OLI image data due to its availability, which coincided with the time series sampling for images for the 2014 and 2024 sampling years.

2.5. Hyperspectral remote sensing of invasive plant species

Hyperspectral imagers, commonly known as imaging spectrometers, provide the advantage of collecting a continuous spectrum over a wide area within the visible and shortwave regions. They accomplish this by employing hundreds of spectral bands with narrow intervals (≤ nm) (Huang & Asner, 2009). The primary advantage of using hyperspectral data is that spectral profiles can be generated for both native and non-native plants, thereby enabling analysis of regions most sensitive to the abundance of the target species (Underwood et al., 2003; Huang & Asner, 2009). Hyperspectral sensors enable the capture of a plant's biochemical composition, closely linking it to species identity by sampling the electromagnetic spectrum in tens to hundreds of bands (Asner & Martin, 2009). For instance, traditional multispectral sensors, such as Landsat, face a significant risk of pixel mixing in heterogeneous landscapes due to poorly positioned bands (Madonsela et al., 2017). According to Mutanga and Skidmore (2004), hyperspectral data provides a solution to mitigate saturation problems typically encountered with multispectral data sensors. Atkinson et al. (2014) state that the development of hyperspectral sensors with enhanced spectral resolution allows for more accurate delineation and classification of invasive plant species based on their biochemical and phenological properties, even in heterogeneous landscapes. Yang and Crews (2020) demonstrated this in their study, which used Landsat-8 OLI to monitor bush encroachment by juniper species in the Texas savanna, revealing that woody cover had increased to approximately 62%. Moreover, a study by Madonsela et al. (2017) utilised a WorldView-2 sensor paired with Spectral Angle Mapper (SAM) to distinguish various tree species in Kruger National Park, South Africa. This approach achieved an overall accuracy of 80.4%, thanks to the interspecies-SAM method, where the (605 nm) band exhibited a statistically significant role in enhancing classification accuracy. Another example is a study by Asner et al. (2007) that examined the distinct canopy hyperspectral signatures of 43 native and alien Hawaiian trees. The reflectance and derivative reflectance signatures obtained using the Airborne Visible and Infrared Spectrometer (AVIRIS) were generally unique compared to those of non-native trees. This distinctiveness in spectral signatures is associated with variations in the measured leaf pigment (chlorophyll). Additionally, Kishore et al. (2024) identified the understory of the invasive species *Lantana camara* and *Chromolaena odorata* in Mudumalai Tiger Reserve, located in the Western Ghats of India, by utilising high-resolution airborne imaging spectroscopy in conjunction with Multiple Endmember Spectral Mixture Analysis (MESMA). The model based on AVIRIS was successful in delineating the understorey of both species (from other identified species) with

an overall accuracy of 87% with root mean square error (RMSE) classification of (0.001 to 0.0025). Recently, Unmanned Aerial Vehicles (UAVs) have been employed in the monitoring and detection of invasive plant species in various regions and ecosystems worldwide (Nowak et al., 2018). An example is a study by Michez et al. (2016b), which used a fixed-wing UAV equipped with two onboard cameras (RGB and RGNIR) to detect and map three invasive riparian species: *Follopia japonica*, *Follopia sachalinensis* (Japanese knotweed), *Impatiens glandulifera* (Himalayan balsam), and *Heracleum mantegazzianum* (Giant hogweed). The UAV images were obtained at different phases, which was done to increase the accuracy of detection as advised by Müllerová et al. (2017). Spectral and texture image metrics were calculated at different scales of image segmentation, based on visible and near-infrared wavelengths.

2.6. Spectral characteristics of invasive plant species

The invasive nature of IPSs in rangelands necessitates the use of advanced remote sensing methods to monitor their spread, as traditional survey methods are costly and time-consuming over large areas. Remote sensing techniques, applied to map, monitor, and quantify the trend of invasion, are made possible by the observed spectral reflectance, which tends to be unique for different vegetation species at various stages of phenology (Joshi et al., 2006). Many IPSs have been classified and successfully distinguished from other vegetation species due to their spectral signatures, which are influenced by biophysical factors (texture, canopy, leaf structure, and orientation) and biochemical factors (chlorophyll and water content) (Royimani et al., 2019). The different reflectance properties of vegetation are determined by the location of the bands in the electromagnetic spectrum of each type of vegetation (Mirik and Ansley, 2012). According to Mutanga and Skidmore (2004), the mapping of IPSs is made possible by remote sensing sensors that are equipped, on board with (i) green bands (wavelength 530 nanometres (nm)-590nm), (ii) near-infrared bands (wavelength 760_nm—890_nm) and (iii) red bands (wavelength 625_nm – 695_nm). Furthermore, newly emerging multispectral sensors, such as Landsat 9 and Sentinel-2, have revealed significant opportunities for vegetation monitoring based on functional types, wherein information is acquired at a broader scale (Shoko & Mutanga, 2017). Several studies have demonstrated that employing hyperspectral sensors with numerous contiguous narrow wavelengths is effective in detecting subtle differences between species (Somers & Asner, 2013b). For instance, the newly introduced Sentinel-2 multispectral imager features an additional red edge band, which has improved its ability to detect IPSs

compared to their counterparts, while Landsat-9 offers improved radiometric resolution. The spectral reflectance of different plant species (predominantly non-native) is distinct in specific spectral wavebands across various seasons of the year, particularly in subtropical and temperate climatic regions (Matongera et al., 2017).

For example, the spectral reflectance of bracken fern makes it difficult to discriminate from grass in the summer season (Royimani, 2019). Most IPSs exhibit reflectance similar to that of other vegetation species during the summer season, when they reach their peak in chlorophyll productivity due to higher sunlight, higher temperatures, and higher soil moisture. As mentioned above, *S. plumosum* grows in large patches of individual shrubs (Avenant, 2015), a characteristic well-suited to remote sensing methods, where the observed patch size can be matched to the image pixel resolution. Its distinct leaf structure and bright-coloured flowers in mature shrubs during the summer season (Snyman, 2009) make it stand out from the co-existing vegetation in the landscape. The canopy characteristics and leaf spectral signatures at the species level will be the basis for discriminating *S. plumosum* in this study. Figure 2 shows the reflectance curve for *S. plumosum* in comparison with grass species, highlighting its significant absorption and reflectance features between 580-758nm and 1095-1422.2nm (Dubula et al., 2016).

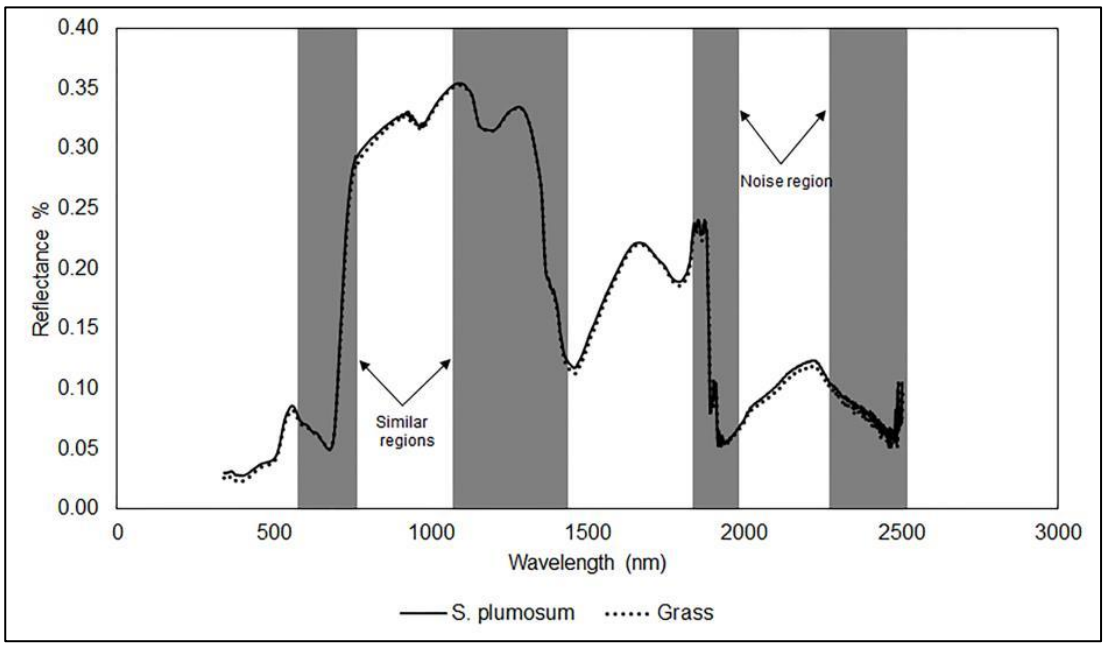


Figure 2: Spectral reflectance of *Seriphium plumosum* in comparison to grass (Adopted from Dubula et al,.2016)

2.7. Machine learning algorithms used to discriminate invasive plant species

In remote sensing, two broad categories of image classifiers are distinguished, namely, supervised and unsupervised classification (Strand, 2006). Due to their nature in data handling, classification tasks are typically performed using either parametric or non-parametric algorithms. The type of classification algorithm used is a significant factor in determining the quality and reliability of the classification output (Lu & Weng, 2007). Various machine learning algorithms (MLAs) have successfully been used in IPSs mapping and detection. Their performance largely depends on, among other things, the nature of the training sample, the quality of information that the sensor can detect, and also on the biophysical features of the landscape in which they are detected (Nath et al., 2014).

Parametric classifiers have been widely used to detect IPSs in many studies, despite reported technical shortcomings, where the classification output is only observed at a pixel level (Fernandez et al., 2015), which distorts accuracy levels, particularly when a low spatial resolution image is being studied (Mather et al., 2022). For example, the maximum likelihood classifier (MLC) is the most commonly used classifier, which assigns each pixel based on its calculated probability of belonging to that class (Mather et al., 2022). Peerbhay et al. (2014) observed that the maximum likelihood classifier notably still performs better than unsupervised methods. The most limiting factor crippling the use of parametric methods for classification is the assumption of the normal or Gaussian distribution of observations, which may not produce favourable results (Huang & Townshend, 2002). Additionally, Matongera et al. (2019) and Lass et al. (2005) reported that parametric classifiers are vulnerable to mixed pixel issues, which are more noticeable in diverse environmental landscapes.

Non-parametric image classifiers, for example, Random Forest (RF), Support Vector Machine (SVM), Classification And Regression Trees (CART), Artificial Neural Networks (ANN) and Naïve Bayes (NB), have been tested in the most recent studies to map IPSs successfully (Bhungeni et al., 2024). Such success is predominantly ascribed to their capacity to consider individual pixels as combinations of pure materials and endmembers within the classification process (Fernandez et al., 2013). Recent advancements in multispectral remote sensing sensors, specifically Landsat 9 (L-9) and Sentinel-2 MSI, have expanded the possibilities for IPS mapping when paired with the aforementioned Machine Learning Algorithms (MLAs), as

noted by Dube et al. (2020). For example, Urban et al. (2021) evaluated the performance of a supervised random forest classifier in predicting *S. plumosum* encroachment in the Free State province of South Africa, utilising multi-year Sentinel-2 data. They achieved an overall accuracy of 80%. A study conducted by Roymani et al. (2017) to determine the multi-temporal distribution of parthenium (*P. Hysterophory L)* in KwaZulu-Natal Province of South Africa used random forest classifier in concert with time series SPOT earth observation data where overall accuracy was (i)71% for 2016 SPOT-6 (ii) 75% for 2012 SPOT-5 (iii) 78% for 2009 SPOT-5 and (iv) 70% for 2006 SPOT-5. Nkhwanana et al. (2022b) compared the performance of RF and SVM, using Sentinel-2 image data, to map *S. plumosum* in a nature reserve in Mpumalanga Province, South Africa. An overall accuracy of 97.42% was achieved for RF and 95.42% for SVM.

Bayable et al. (2023) evaluated the performance of RF, SVM, and CART for detecting and estimating the seasonal and spatial coverage of water hyacinth (Eichhornia crassipes) in Lake Tana, Ethiopia, using Landsat-8 and Sentinel-2 imagery. The maximum coverage area of *E crassipes* observed in autumn was 22.4 km², compared to 2.2 km² that was observed in summer. A noticeable variation was also reported, indicating a 62.5% decrease from winter to spring and a significant 81.7% increase from summer to autumn. The RF method was reported to be more accurate, with accuracy ranging from 97% to 100%, albeit by a minimal margin, when compared to other classifiers. Another study by Sharifipour et al. (2023) in Qurveh, Iran, utilised SVM, RF, ANN, CART, and NB machine learning algorithms to map 185 rangeland species. The NB algorithm achieved the highest stable and consistent performance across all species with the area under the curve (AUC) of 0.782. The following UACs were reported for the other algorithms, namely SVM (UAC = 0.763), ANN (UAC = 0.762), CART (UAC = 0.627), and BN (UAC = 0.617). Recently, Mtyoba and Shoko (2024) successfully utilized the random forest in conjunction with the MaxEnt species distribution model and Sentinel-2 image data to map and model Lantana camara in the province of Mpumalanga, South Africa, achieving user's and producer's accuracies of 91% and 84%, respectively.

2.8. The use of species distribution models in invasive plant species ecology

Species Distribution Models (SDMs) are a collection of tools and methods used in ecological and geographical contexts to examine species distribution and their relationships with the physical environment (Whittaker et al., 1973). SDMs are increasingly employed in the fields

of ecology and conservation research to effectively map and predict ecosystems that are vulnerable to encroachment by both native and non-native plant species. It is a combination of tools used for predictive analysis of species distribution variability, providing a quantitative baseline to inform conservation policies and support decision-making (Rios et al., 2024). Recently, the future distributions of species have been mapped and predicted using SDMs alongside Ecological Niche Models (ENMs), as noted by Fourcade et al. (2014). The SDMs connect environmental variables to established species occurrence sites, identifying abiotic factors that support species distribution in new or existing locations. According to Phillips et al. (2006), the maximum entropy (MaxEnt) model has become the preferred option among various SDMs because of its superior predictive performance, and as such, it has proven to be more popular in more recent API studies with great success.

A study conducted by Adepoju et al. (2020) in the protected mountainous grasslands of the Free State Province of South Africa used environmental variables such as temperature, rainfall, topography, and vegetation as continuous predictor variables in the MaxEnt model to monitor grassland encroachment by *S. plumosum*. A positive AUC value of 0.876, representing the estimated probability of species occurrence, was obtained, indicating a good model fit. The study noted that temperature and fire events are the primary factors influencing the distribution pattern of *S. plumosum.* Ngarega et al. (2021) mapped the geographical range of appropriate habitats for mopane trees (*C. mopane*) in Southern Africa using the MaxEnt model. The study concluded that the distribution of *C. mopane* is mainly influenced by solar radiation, annual temperature range, and general annual precipitation. Furthermore, the study reported that suitable habitat areas are likely to expand by 4.08% to 4.46% and decline by 8.83% to 10.08%. Most recently, a study conducted by Mtyobila and Shoko (2024) utilised MaxEnt to model *Lantana camara* in the province of Mpumalanga, South Africa. The study concluded that the elevation variable was the most responsible and influential factor driving the spread of *L. camara*, with a predictive accuracy of 0.88.

2.9. Cloud computing platforms used in the remote sensing of invasive plant species

The application of Remote Sensing (RS) and Geographic Information Science (GISc) in recent years has increasingly used Cloud-Based Computing platforms, such as Google Earth Engine (GEE), Microsoft Planetary Computer (MPC), and Amazon Web Services (AWS), among

others. The use of these platforms offers numerous benefits for processing RS data, which was previously nearly impossible, thereby enabling online, on-demand, and scalable processing capabilities that traditional RS platforms cannot achieve (Kaur et al., 2023). GEE has become an essential tool in vegetation remote sensing, offering seamless access to a vast satellite image database and advanced image classification algorithms (Masemola et al., 2020). Recently, GEE has enhanced access to much-needed image data libraries and machine learning algorithms, enabling statistical analysis and data modelling for advanced interpretation of land use and land cover change. For example, studies conducted by Shoko and Ndlovu (2023) and Mtyola and Shoko (2024) serve as a testament to the fusion of such models with multi-spectral image data for mapping invasive plant species and monitoring land cover change. These studies were conducted using the Google Earth Engine (GEE) platform for post-data processing and the implementation of a machine learning algorithm. More recently, Bhungeni et al. (2024) utilised the GEE cloud computing platform to evaluate and compare various machine learning algorithms for mapping LULC in the province of KwaZulu-Natal, with all accuracy test results exceeding 80%. Urban et al. (2021) used the combined Synthetic Aperture Radar (SAR) (Sentinel-1) and optical (Sentinel-2) Earth observation information to predict *S. plumosum* encroachment in conjunction with RF as a supervised classifier for a period between 2015 and 2020.

2.10. Conclusion

The reviewed literature demonstrates the usefulness of various remote sensing data in monitoring native or non-native invasive plant species. The literature indicates that earlier versions of multispectral data from ASTER, Landsat, and SPOT had limited resolution, including radiometric and spectral, which were significant limitations for detecting invasive plant species. Recent advancements, such as the introduction of Sentinel-2, Landsat-8/9, and SPOT-6/7, have improved spatial, spectral, and temporal resolution, thereby bridging a significant gap that older sensors previously failed to address. Many studies have confirmed that this has provided additional capabilities, including improved radio-metric resolution and an additional red edge band, for example, which enhance the detection of invasive plant species. Significant challenges for detecting invasive plant species are also associated with phenology, spectral characteristics, and environmental heterogeneity. The availability of high-resolution (five metres or finer) remains out of reach due to cost and is a major limiting factor. The most helpful approach, perhaps, for biodiversity monitoring studies remains a compromise

between cost and accuracy that can be achieved from intermediate resolution provided by either Landsat or SPOT image data sets. The literature further reveals that the use of machine learning algorithms, such as RF, SVM, and CART, in conjunction with commonly used indices, for example, NDVI, NDWI, BSI, and SAVI, has proven to be a robust and invaluable tool to aid, with precision, the classification of remotely sensed data. Machine learning ensembles easily integrate with cloud computing platforms such as GEE, providing direct access to image data catalogues. Many studies have proved this to be a game-changer in analysing and interpreting change detection.

CHAPTER THREE: MATERIALS AND METHODS

3.1. Introduction

This chapter outlines the methods used to achieve the study's aims and address its questions. It describes the procedures for acquiring and preparing Landsat images, MaxEnt modelling data, as well as the subsequent Land Use and Land Cover (LULC) classification using a random forest machine learning algorithm.

3.2. Study Area

The study area is located under the Nquthu Local Municipality outside the Nquthu Town, Province of KwaZulu-Natal, South Africa. The rangeland area incorporates the villages of Vansdrift, Jabavu, and Masotsheni. It lies within the latitudes 28, 1760695°S and 28, 3176555°S and longitudes of 30, 6586788°E and 30, 6239474°E and covers about 597 km^2 of space. The Nquthu town is the nearby urban centre and the central economic zone of the municipality (Figure 3). The region features diverse landscapes, including vast grasslands and shrublands in the northern part, with occasional native forest stands and water bodies. The biophysical properties of the area are defined by undulating landscapes, gentle slopes, and hills located in the southeastern part, characterised by rock outcrops that shape its unique geological character. According to Clark et al. (2009), the altitude across the study region varies from 0 to 1750 m above sea level. The western boundary of the area is defined by the regional uMzinyathi River, which serves as the primary source of water for both livestock and human consumption (Namugize et al., 2018).

The daily average temperature ranges from 23 °C to 31 °C in summer (October to March) and from 13 °C to 21 °C in winter (April to September). The mean annual rainfall is approximately 600-800 mm, with the majority falling during the summer months (October to March). Besides the apparent dominance of the *S. plumosum* infestations forming a shrubland layer almost in the central part, other land use and cover classes include crop plantations, such as maise, bare land or degraded land, built-up areas, seasonal water bodies, wetlands, rivers, and grassland, as per the official description provided by the Department of Rural Development and Land Reform (2017). There is a notable increase in built-up and degraded or bare land areas as a land cover class, resulting in a general decrease in natural vegetation across the region.

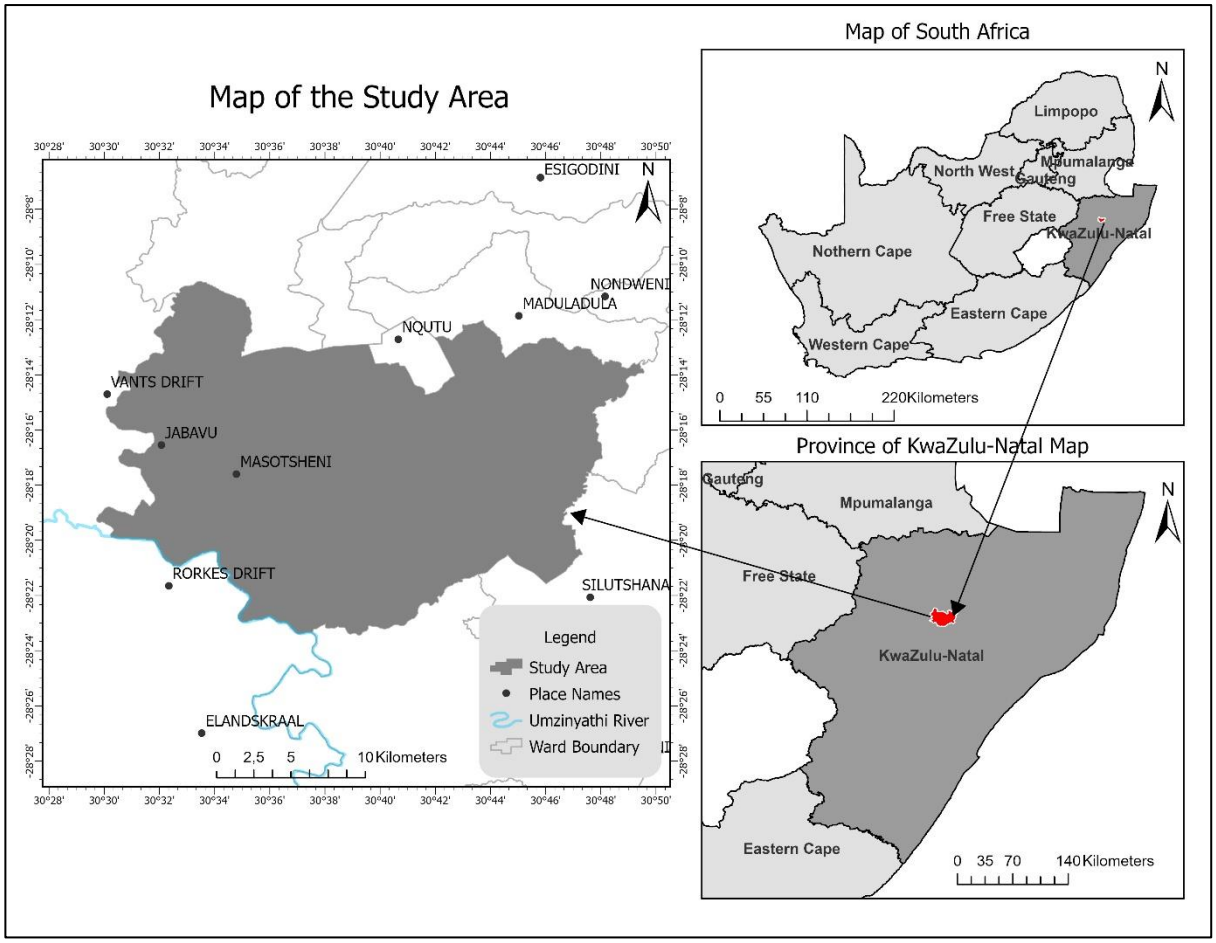


Figure 3: Locality map of the study area within Nquthu Local Municipality in KwaZulu-Natal Province, South Africa.

3.3. Collection of field reference data

Field data were collected during visits in the summer months of January, February, and March 2025. The purpose of the visit was to identify the standard land cover classes that are dominant in the area, including *S. plumosum.* A total of eight thematic land cover classes were identified, namely water, grassland, built-up, natural forest, *S. plumosum,* bare land (degraded land), shrubland, forest plantations and cropland (Table 1). Field data were subsequently collected using a Trimble Global Positioning System (GPS) device with sub-meter positional accuracy, in conjunction with the Trimble Terraflex application. Random sampling, combined with the purposive sampling method, was employed, where all surveyed plots of *S. plumosum* measured 30 m x 30 m to match the 30 m x 30 m spatial resolution of the Landsat-8 OLI image. A total of 570 points were collected and recorded for both naturally clustered populations and isolated individual shrubs located within a 1 m buffer width of each plot of *S. plumosum*.

Table 1: Summary and general description of the standard land cover classes used in the study, source: South African National Land Cover (SANLC 2016).

Class Code	Class Name	Description
1	Natural Forest	Areas dominated by indigenous forest species with closed canopy cover.
2	Shrubland	Regions covered with low-growing woody plants, including fynbos and karoo.
3	Grassland	Areas primarily covered with grasses, with minimal tree or shrub presence.
5	Waterbody	Permanent or seasonal bodies of water, including rivers, lakes, and dams.
6	Cropland	Areas used for agriculture, including commercial and subsistence farming.
7	Built-up Area	Regions with human-made structures, including residential, commercial, and industrial areas.
8	Bare land	Partial vegetated areas, bare land due to either erosion, natural degradation or human factors, post-harvest crop fields, dry riverbanks, and stripped rock areas.
9	Forest Plantation	Areas planted with tree species for commercial purposes, such as timber production.

Furthermore, a total of 370 ground truth points for the other seven (7) identified thematic classes were collected as additional training points and were used to derive pixel-based training samples as polygons for each class within Google Earth Engine Pro (GEEP). Collected GPS points were downloaded from the Trimble Connect application and imported as a point shapefile in ESRI ArcGIS Pro version 3.4. A time slider was used to select a date corresponding to the image, visually confirming the presence of identified classes for both 2014 and 2024 images. The collected GPS points were then imported as a comma-separated values (.CSV) file and overlaid on the image to locate the occurrences of different classes within GEEP. Polygons

representing the corresponding land cover classes were then digitised for each land cover class using the collected locality points as a guide. This was done to enhance the accuracy of the classification algorithm to discriminate *S. plumosum* from other common species, especially grass species. The totals for all pixels in a polygon, per class (70% for the training split and 30% for the validation split), were calculated using Python within Google Colab using *scikit-learn* (*from sklearn.model_selection import train_test_split*). This method was previously employed by Nkhwanana et al. (2022a) to map *S. plumosum* in the province of Mpumalanga, South Africa, yielding accurate and reliable modelling results. The same *S. plumosum* points were later used as input "presence points" to train the MaxEnt species distribution model to predict habitat suitability for the *S. plumosum* for both current and future scenarios.

Table 2: Training and validation samples for each 2014 image data.

Total Pixel		**2014 Training and Validation Sample**	
LULC Classes	**Samples (*N*)**	**Train Set (70%)**	**Validation Set (30%)**
Water	40	26	14
Grassland	4245	2975	1270
Built-up	145	104	41
S.plumosum	1638	1168	470
Forest	2339	1596	743
Bareland	563	406	157
Cropland	15411	10815	4596
Shrubland	855	587	268

Table 3: Training and validation samples for each 2024 image data.

Total Pixels		**2024 Training and Validation Sample**	
LULC Classes	**Samples (*N*)**	**Train Set (70%)**	**Validation Set (30%)**
Water	26	18	8
Grassland	3452	2416	1036
Built-up	176	123	53
S.plumosum	2456	1719	737
Forest	2150	1505	645
Bareland	726	508	218
Cropland	14311	10018	4293
Shrubland	625	438	187

3.4. Image data collection

The study utilised Landsat 8 OLI images. The two Landsat multispectral images for 2014 and 2024 (10-year period) were obtained from the Copernicus Open Hub (https://scihub.copernicus.eu/), which is the GEE data catalogue from the publicly available GEE Data library with level 2 surface reflectance. Landsat-8 OLI image data were chosen for this study because their availability coincided with the study period: the satellite was launched in 2013, and clear, ready-to-use images were available in 2014. It has a proven track record in the literature for monitoring land-use and land-cover change, which was an advantage for this study. The advantage of the reflectance category is that images are almost ready for analysis with minimal pre-processing, such as radiometric and atmospheric corrections (Kaur et al., 2021). Both image dates were in March 2014 and 2024, and the which coincide with the field data collection dates, when encroachment was at the maturity stage. The image's spatial and spectral characteristics are summarised in Table 4. Images from various dates within the same season were obtained using Ee.filter date. The study area boundary polygon shape, known as the region of interest (ROI) file, was used to create a subset from the composite image using the *Clip ()* function with GEE. The *metadata* function was then used to select only scenes with cloud cover below 10%, utilising the CFmasking function to remove cloud contamination in the image, where zero values are assigned to pixels affected by cloud cover (Mashala et al., 2023; Floreano & De Moraes, 2021). We then set the *EE filter* functions to select image data with cloud cover of 10% or less for our study purposes. From the series of image scenes within a specified period (January to March), we then selected the medium composite of all images.

Table 4: Landsat 8-OLI spatial and spectral characteristics and their resolutions. Source: NASA Landsat Science (2025).

Bands	**Wavelength (λ)**	**Resolution (m)**
Blue	0.45–0.51µm	30 m
Green	0.53–0.59 µm	30 m
Red	0.64–0.67 µm	30 m
Near Infrared (NIR)	0.85–0.87 µm	30 m
Shortwave Infrared 1 (SWIR 1)	1.56–1.65 µm	30 m
Shortwave Infrared 2 (SWIR 2)	2.10–2.29 µm	30 m

3.5. Image classification using Random Forest

For this exercise, the random forest (RF) was chosen to perform image classification of all identified land cover classes and detect associated changes. RF was selected for this study due to its ability to utilise several models as an ensemble (Breiman, 2001), a feature that multiple studies have proven to be its main advantage in outperforming other algorithms. The RF model is a group of classifiers that resembles a tree structure where several trees are generated using a training sample as a subset and by randomly selecting variables per sample (Breiman, 2001). Individual trees then produce classification results after being trained on original data subsets (Mananze et al., 2020). A majority vote is cast to produce the final classification result (Breiman, 2001). Its results are stable because it utilizes several trees, thus reducing the risk of overfitting, which is a common problem in many algorithms (Odindi et al., 2016). Its primary strength arises from its unique classification approach, which requires reduced data processing resources, such as high-performance computer GPUs, and time, while effectively handling high data dimensionality (Orieschnig et al., 2021). RF was accessed directly within the GEE web-based IDE in the code editor console using the *ee.Classifier.smileRandomForest* command from the GEE library. The model parameters were set with *ntree* at 25 and *mtry* at 2 leaves for all image bands (6 multispectral and 3 additional spectral indices) as explanatory variables. Essentially, *mtry* indicates the number of explanatory variables per split, while *ntree* denotes the number of decision trees to be planted. As mentioned, the collected reference points and polygons were geo-rectified and imported into GEE, overlaid onto each image as the classification reference data (Carlotto et al., 2009). The GEE script was connected to Google Collaboratory (Google Colab) as a Python script in a Jupyter notebook, which was the preferred post-processing language for our purposes due to its ease of visualisation and manipulation. The Jupyter notebook is based on the *geemap* Python package, which utilises the Python API for interactive mapping and submits computational requests directly to the Earth Engine servers (Chen et al., 2023). This enabled the visualisation and interaction with the Earth Engine server using Python instead of JavaScript.

3.6. Classification accuracy assessment

The reclassification results were validated using a confusion matrix for both images (2014 and 2024), calculated with the *errorMatrix* command, which determined the overall accuracy (OA), user accuracy (UA), and producer's accuracy (PA). Ultimately, a Kappa coefficient was calculated for the RF model results in both images, with values ranging from -1 to 1 to rank

the classification accuracy of the image, where ≤0.40 indicates fair performance, ≤0.75 indicates satisfactory performance, and ≤1 indicates good model performance.

3.7.Extraction of spectral indices

To improve the classification accuracy and identification of different LULC classes from the image, spectral indices were derived from the Landsat-8 image using Python within a Google Colab Jupyter notebook. In this study, the Normalized Difference Vegetation Index (NDVI) for vegetation, the Normalized Difference Water Index (NDWI) for water, and the Bare Soil Index (BSI) for soil or bare land were chosen based on their importance in minimizing the effect of soil background and enhancing vegetation greenness. They were then added as variables for image classification to supplement the raw multispectral bands of the Landsat-8 OLI and were incorporated as input features into the SHAP model. Spectral indices are derived pixel-wise ratios of two or more bands of a multispectral image (Orieschnig et al., 2021), which can be used to enhance classification of diverse spatial attributes from similar class members (Bhungeni et al.,2024) to better represent spatio-temporal variations in vegetation, water and soil surfaces and their correlations with key climatic factors. The selected indices are based on the spectral reflectance characteristics in the visible, NIR and SWIR bands. According to Rouse (1974), NDVI quantifies vegetation with the difference between near-infrared (which is reflected by vegetation) and red light (which is absorbed by vegetation). BSI integrates the blue, red NIR and SWIR bands to detect the soil variations (Kitimaru et al., 2002). The SWIR and red bands quantify the soil mineral composition, while the blue and NIR spectral bands enhance the presence of vegetation. According to McFeeters (2007), NDWI utilizes reflected near-infrared radiation and visible green light to enhance the presence of features while suppressing the presence of soil and vegetation features. The selected indices were calculated using the following equations in Table 5.

Table 5: Indices selected to supplement raw spectral image bands for classification.

Index	Python Expression	Equation	Reference
BSI	*var bsi = image.expression()*	$BSI = \frac{((Red+SWIR) - (NIR+Blue))}{((Red+SWIR)+ (NIR+Blue))}$	*Rikimaru et al., (2002)*
NDWI	*var ndwi = image.expression()*	$NDWI = \frac{Green - NIR}{Green+ NIR}$	*McFeeters (1996)*
NDVI	*var ndvi = image.expression()*	$NDVI = \frac{NIR - Red}{Red+NIR}$	*Rouse et al., (1974)*

3.8. Implementation of SHaply Additive exPlanations.

SHaply Addictive exPlanations (SHAP) is described by Lungberg and Lee (2017) as a method used to explain the contribution of each feature to the final prediction. This is achieved by applying game theory concepts to illustrate how each feature influences a machine learning model's prediction. The study assessed the band performance, or the contribution of each feature within each class to the model prediction, by averaging its marginal contribution across all combinations using the SHAP method in Google Colab Notebook. For this, the *Sci-Kit Learn* and SHAP packages within Google Colab were imported to build the value explainer model, which computes the feature importance values that vary for each feature (Chen et al., 2023). The importance and impact of each input variable for each classifier (RF) were assessed and ranked using the SHAP algorithm, which calculates the average of the absolute Shapley values. The feature output is illustrated using a bar chart, where features positioned higher on the chart indicate a greater contribution to the model prediction. The SHAP model is expressed by the following equation (Lundberg & Lee, 2017):

$$\phi i = \sum_{S \subseteq N\{i\}} \frac{|S|!(|N|-|S|-1)!}{|N|!} [fs \cup \{i\}(xs \cup \{i\}) - fs(xs) \qquad (1)$$

Where:

$\boldsymbol{N}$: Set of all features.

$\boldsymbol{S}$: Subset of features not including feature i.

$|\boldsymbol{S}|$: Size of the subset $\boldsymbol{S}$.

$\boldsymbol{f}s(xs)$: Model output using only features in subset $\boldsymbol{S}$.

$\boldsymbol{f}s \cup \{i\}(xs \cup \{i\})$: Model output using $\boldsymbol{S}$ plus feature i.

ϕi: SHAP value for feature i – its contribution to the final prediction

3.9.Application of the Species Distribution Model

3.9.1. Bioclimatic data acquisition and processing

Bioclimatic data were obtained in raster format (geo.tif) from WorldClim (www.worldclim.org) for both the current (WorldClim v2.1: 1970-2000 and future WorldClim v2.1: 2021-2040) climate (temperature and precipitation), with a resolution of approximately 30 arc seconds (1 km^2). Model raster data based on the Medium-resolution Beijing Climate Centre Climate System Model (BCC-CSM2-MR) ssp126 circulation model for the period 1970-2000 were utilised to model the current suitability scenario. For the future habitat suitability prediction,

the period 2021-2040 was selected from the same data model. All selected bioclimatic variables for the model were free from multicollinearity after a positive Pearson correlation test with a correlation coefficient (γ) larger than 0.8, which were most fitting for the model. Variables with (γ) ≥ 0.8 were subsequently excluded to improve model performance with no influence of multicollinearity. All suitable variables are listed in Table 6, and the chosen predictors for this study are highlighted in bold. Additional topographic variables used were i) elevation, ii) slope, and iii) topographic position index (TPI), and all were derived from a digital elevation model (DEM) using the Spatial Analyst tool in ArcGIS Pro version 3.4. All variables were resampled to match the spatial resolution of the topographic variables and extracted to the study area boundary using the Extract Raster function in ArcGIS Pro version 3.4. Finally, all extracted raster data were converted from geo.tif to ASCII format using the Raster to ASCII command, which is a format suitable for the MaxEnt model application. Converted files were imported as environmental variables within the MaxEnt model. Lastly, the *S. plumosum* data points (GPS) were imported as samples (species presence) to perform the main species distribution modelling using Maxent version 3.4.4, a stand-alone Java application.

Table 6: Description of bioclimatic variables used for MaxEnt model prediction sourced from Fick et al., (2017).

Code	Environmental variables	Units
Bio1*	**Annual Mean Temperature**	**℃**
Bio2*	**Mean Diurnal Range**	**℃**
Bio3	Isothermally (BIO2/BIO7) (* 100)	%
Bio4*	**Temperature Seasonality (standard deviation *100)**	**%**
Bio5	Maximum Temperature of Warmest Month	**℃**
Bio6	Minimum Temperature of Coldest Month	**℃**
Bio7*	**Temperature Annual Range (Bio5-Bio6)**	**℃**
Bio8*	**Mean Temperature of Wettest Quarter**	**℃**
Bio9*	**Mean Temperature of Driest Quarter**	**℃**
Bio10	Mean Temperature of Warmest Quarter	**℃**
Bio11*	**Mean Temperature of Coldest Quarter**	**℃**
Bio12*	**Annual Precipitation**	**mm**

Bio13*	**Precipitation of Wettest Period**	**mm**
Bio14	**Precipitation of Driest Period**	**mm**
Bio15	Precipitation Seasonality (coefficient of variation)	%
Bio16	Precipitation of Wettest Quarter	mm
Bio17	Precipitation of Driest Quarter	mm
Bio18*	**Precipitation of Warmest Quarter**	mm
Bio19*	**Precipitation of Coldest Quarter**	mm

Note: * Bold text indicates the bioclimatic variables used for the model.

3.9.2. Maximum Entropy model implementation and performance validation procedure

The Maximum Entropy (MaxEnt) model version 3.4.4, which can be accessed for free (https://biodiversityinformatics.amnh.org/open_source/maxent/), was used to model the current and future habitat suitability for the *S. plumosum*. MaxEnt utilises presence-only occurrence data in conjunction with environmental variables to estimate the probability of occurrence or potential suitability of habitats. To achieve this, the species modeling data points were split into training and testing sets using a 70:30 ratio, with 1000 points generated as background. This means that modelling was done using 70% of the observed points for parameter estimation (suitability modelling), while the remaining 30% was used for model validation. Bootstrap was selected as a method for replication and cross-validation, along with jackknife, to evaluate the performance of each variable within the model, utilising the test and train gains as input parameters. Other model settings were left at their default values except for iteration tuning, which was set to 500 with 10-fold cross-validation to estimate the ensemble mean.

The occurrence data for model accuracy were evaluated using the receiver operating characteristic (ROC) curve and area under the curve (AUC), due to its ability to display the proportions of actual positives and true negatives (Cord et al., 2013). This is the estimated probability of a randomly chosen grid cell in a correctly adjusted model and serves to define the model's success. AUC values were examined using the test points; values less than 0.8 indicate poor model performance, while those above 0.9 are considered optimal for model performance (AUC $\geq$ 0.9 = very good, 0.9 > AUC $\geq$ 0.8 = good, and AUC < 0.8 = poor)

according to Shabani et al., (2020) and Vilà' et al., (2012). The performance omission rate evaluated the model's low overfitting during training and testing, a notable strength of SDMs, where overfitting is minimised and discriminatory ability is high (Ngarega et al., 2021a). The best model was selected based on the input parameters and the resulting map. For further cross-validation and analysis, the Presence-Only Prediction (Spatial Analyst) tool within ArcGIS Pro version 3.4 was used to compare results and for enhanced mapping functionality and outputs, where the same variables were used to train the prediction model. Figure 4 shows the project workflow conceptual chart from data collection, pre- and post-processing, to classification results.

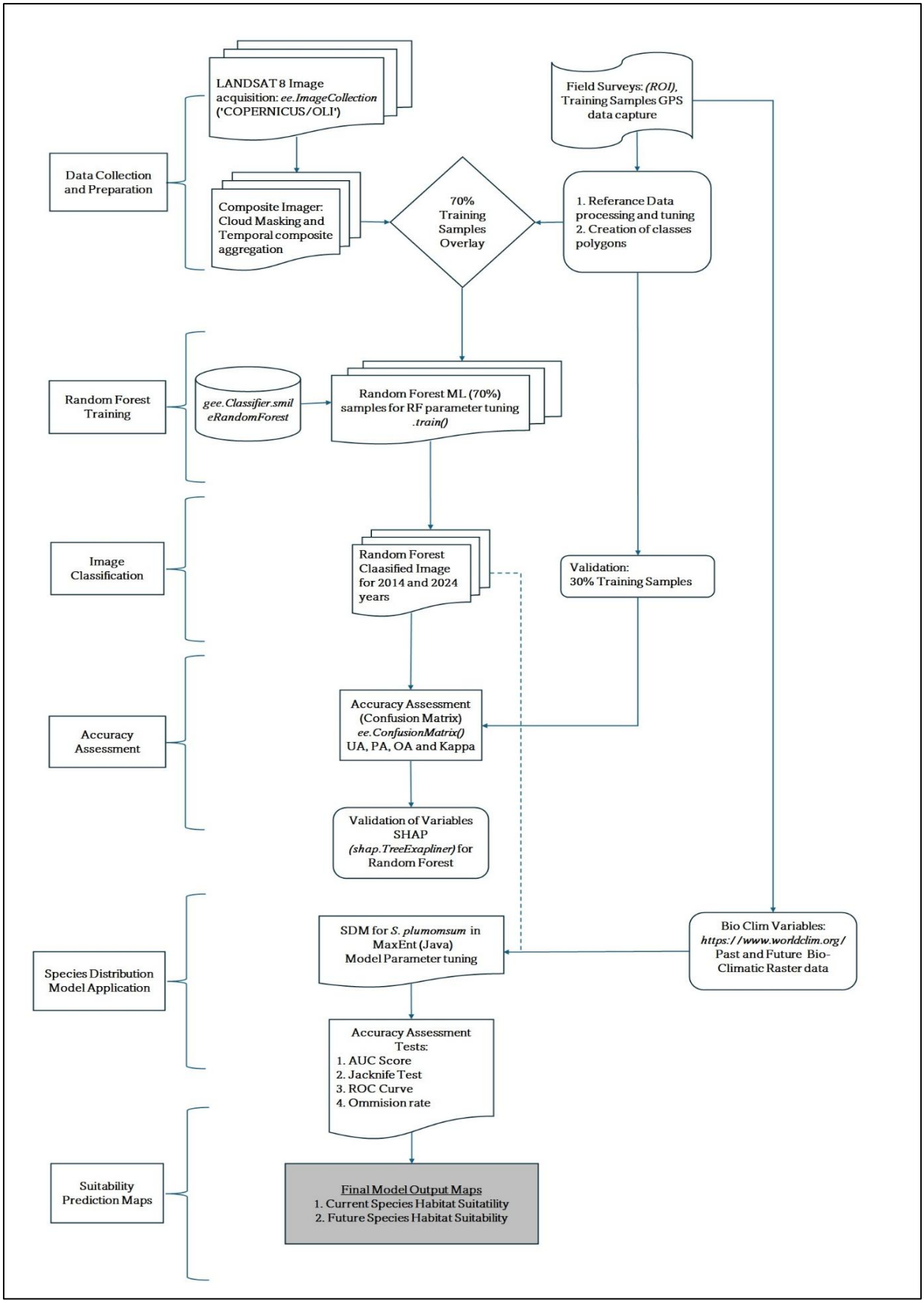


Figure 4: Methodology workflow conceptual chart.

CHAPTER FOUR: RESULTS

4.1. Introduction

The project aimed to monitor the invasive species *S. plumosum* through spatial and temporal analysis to understand the dynamics and environmental variables contributing to its distribution. To achieve this, a time series from 2014 to 2024 and a predictive analysis method were implemented and tested. Various land cover classes prominent in the study area were identified and comparatively analysed over a ten-year period. Furthermore, the study utilised bioclimatic variables to identify the primary drivers of land invasion by the target species over a specified period. Finally, all results uncovered by the two models implemented in the study are presented and analysed in this chapter.

4.2. Image classification accuracy assessment

The random forest model was trained and tested using the Landsat imagery. The results revealed that machine learning techniques successfully mapped all classes in both years across varying environmental heterogeneity (Figure 5). Only 30% of the sample size was used for validation. Producer accuracy (PA), overall accuracy (OA), user accuracy (UA), and kappa coefficient were calculated to assess the performance of each model. The model achieved PA and OA of 90.1% and 88.1% in 2014, and 93.5% and 77.7% in 2024, and kappa coefficients of 0.84 and 0.87 were obtained for both models (Table 7), indicating strong agreement (>80). The land cover class of interest (*S. plumosum*) for this study achieved a PA of 71% and UA of 87% for 2014, and 83% and 93% for the 2024 classification accuracies, respectively. These values serve as good indicators of random forest performance when combined with the Landsat-8 OLI image, enabling the discrimination of *S. plumosum* from other similar spectral reflectance curves, such as those of grass and other shrub species.

Table 7: Confusion matrix for A) 2014 and B) 2024 accuracy assessment of LULC.

A) 2014 Image: Assessment Matrix

LULC Classes	Water	Grassland	Builtup	S. plumosum	Forest	Bareland	Cropland	Shrubland	PA%	UA%
Water	13	0	0	0	0	0	0	1	0.9286	0.8125
Grassland	0	979	0	26	1	5	259	0	0.7709	0.8718
Builtup	2	2	13	0	0	1	23	0	0.3171	0.8667
S.plumosum	0	53	0	334	0	0	83	0	0.7106	0.8766
Forest	0	2	0	0	696	0	18	27	0.9367	0.9342
Bareland	0	1	2	1	0	131	20	2	0.8344	0.9097
Cropland	1	84	0	20	3	7	4476	5	0.9739	0.9155
Shrubland	0	2	0	0	45	0	10	211	0.7873	0.8577
Sum	16	1123	15	381	745	144	4889	246		
Overall Accuracy %	90.1									
Kappa	0.84									

B) 2024 Image: Accuracy Assessment Matrix

LULC Classes	Water	Grassland	Builtup	S. plumosum	Forest	Bareland	Cropland	Shrubland	PA%	UA%
Water	10	1	0	0	0	2	0	5	0.5556	1.0
Grassland	0	1121	2	12	1	0	119	1	0.8925	0.9099
Builtup	0	5	19	0	1	4	17	0	0.413	0.6786
S.plumosum	0	22	0	398	0	1	54	0	0.8379	0.9321
Forest	0	3	1	0	651	0	0	32	0.9476	0.9105
Bareland	0	7	1	0	0	147	12	4	0.8596	0.9245
Cropland	0	69	5	17	4	4	4528	8	0.9769	0.9549
Shrubland	0	4	0	0	58	1	12	171	0.6951	0.7738
Sum	10	1232	28	427	715	159	4742	221		
Overall Accuracy %	93.5									
Kappa	0.87									

4.3. Land use and land cover change detection

The change in area coverage for each class was mapped and calculated, which shows that *S. plumosum* encroachment significantly increased between 2014 and 2024 (Figure 5). The land area covered by each class was calculated in square kilometres (km²), along with the percentage increase or decrease for analysis (Figures 6 and 7). *S. plumosum*, as a land cover class, invaded approximately 20 km² (3.4%) of land in 2014 and increased to cover 74 km² (12.4%) of land by 2024, representing a significant change of about 54 km² (9%) of land. It is distributed evenly across the study area, with both mature canopy clusters and isolated shrubland, mainly on gently sloping surfaces. The density decreases notably in the central interior towards the western boundary, with scattered patches of new encroachment. The distribution decreased from around a 15% slope onward, particularly in steep-slope and high-TPI sections. In the 2014 image (Figure 5A), the invasion was primarily dominant in the northwestern part of the area, with small patches towards the southeast. Observed in the 2024 image (Figure 5B) is an increased extent of invasion in more mature clusters, which are spread across the study site, particularly towards the southeast.

Cropland was also a key land cover class, accounting for the majority of land use in the area, covering 370 km² (62%) in 2014. However, it showed a decline of 54.6 km^2 (-7.4%) in 2024. Water bodies (dams, rivers, and streams) are a dynamic class influenced by weather patterns and seasonality, and their area declined from 7 km² (1.2%) to 3 km² (0.3%), while built-up areas increased from 5 km² (0.5%) to 22 km² (3.7%). Other observed changes exhibited by other classes, such as built-up areas and water bodies (man-made dams and pans) showed insignificant fluctuations during the same period.

Grassland cover occupied 92 km² in 2014 (15.4%) of the land but decreased to 79 km² (8.2%) in 2024, noticeably, while *S. plumosum* increased in the same period. The natural forest decreased from 35 km² (5.9%) to 16 km² (2.7%), and the shrubland decreased from 39 km² (6.5%) to 27 km² (4.5%), resulting in a significant decline in land area coverage. In comparison, bare or degraded land increased by 51 km^2 (8.5%) from 29 km^2 (4.9%) to 80 km^2 (13.4%) in the same period.

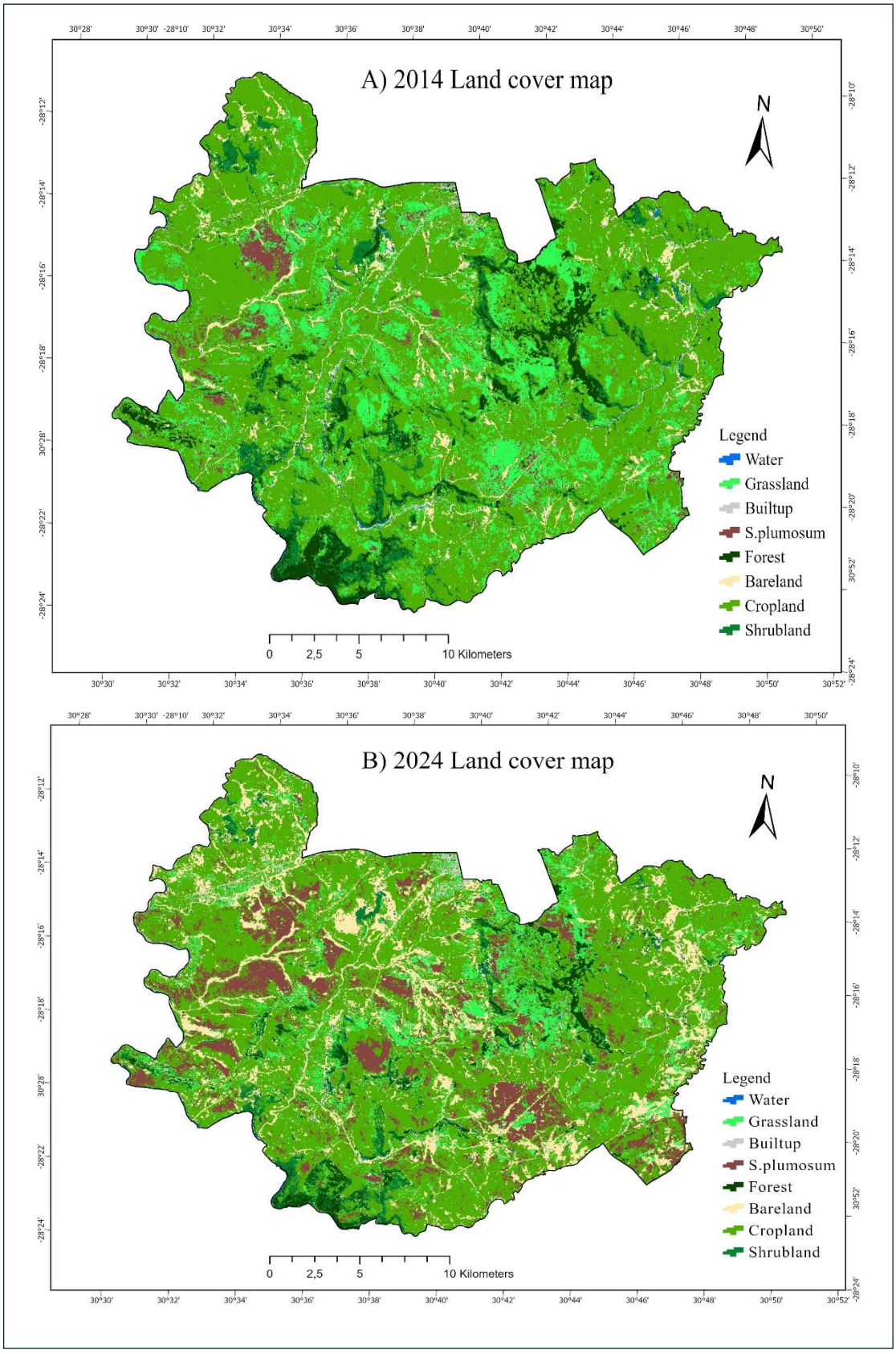


Figure 5: RF classified image: A) for 2014 and B) for 2024 showing land use and land cover (LULC) in the study area located in the Nquthu Municipal area, KwaZulu-Natal, South Africa

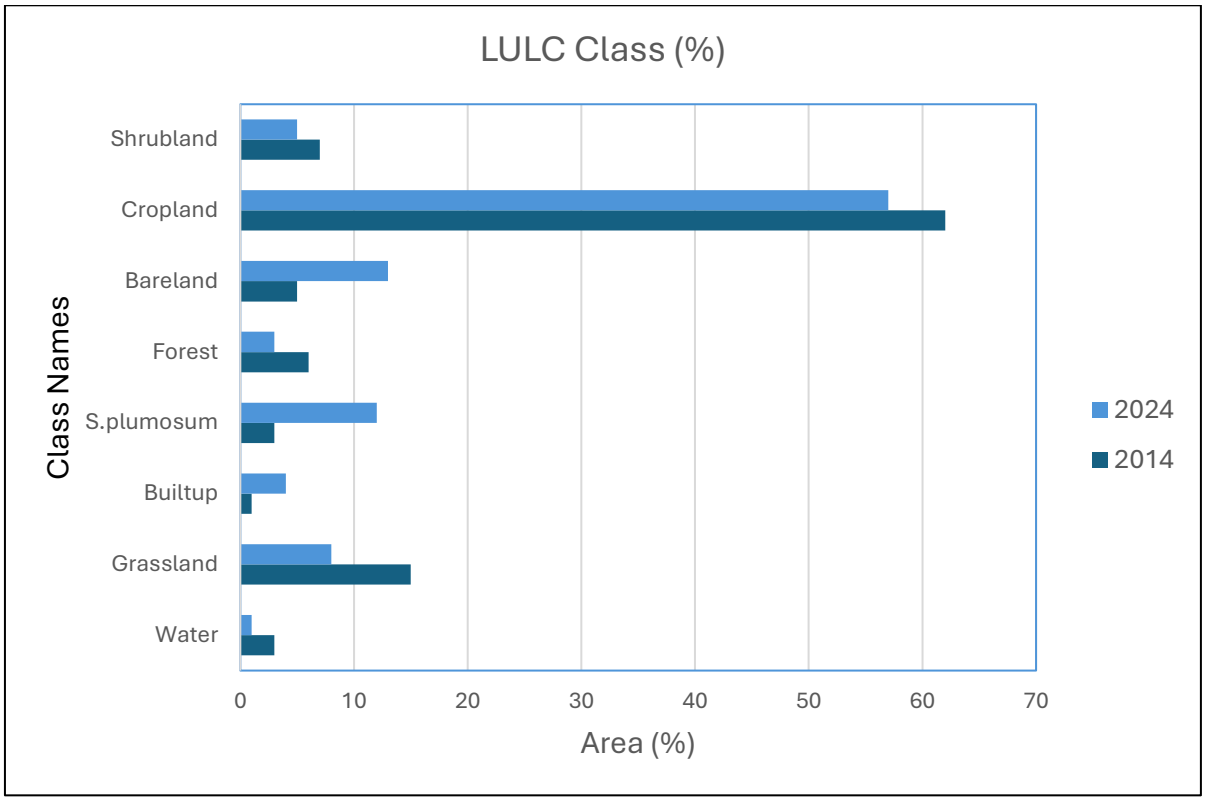


Figure 6: Land Use and Land Cover (LULC) change (%) for different classes in the study area located in the Nquthu Municipal area, KwaZulu-Natal, South Africa.

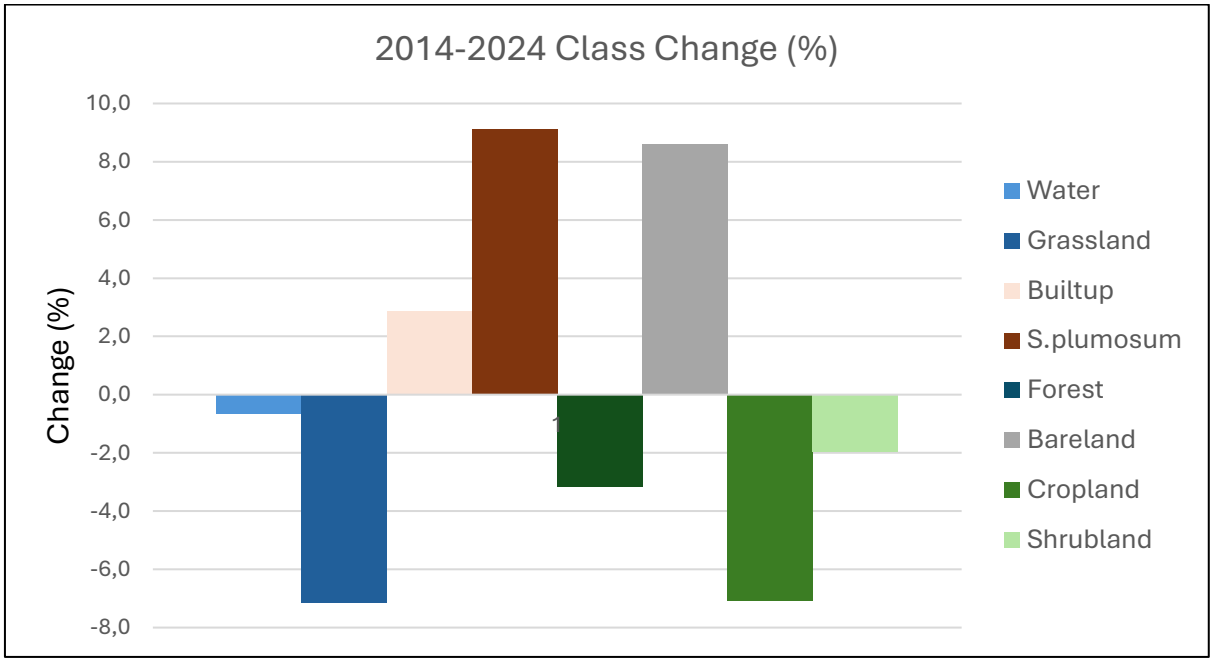


Figure 7: Calculated changes per class LULC class showing class increases and decreases in the study area located in the Nquthu Municipal area, KwaZulu-Natal, South Africa.

4.4. Measurement of Random Forest model variable feature importance

The study used Landsat-8 OLI multispectral bands to map multiple LULC classes in the study area. The contribution or impact of each variable (band) was evaluated based on the average of its SHAP absolute value. The model results are presented as bar plots to assess the overall importance of each image (Figure 8A and 8 B). The contribution of each feature or its importance is measured on the y-axis and is explained by the length of the bar it represents, whilst the average SHAP values are represented on the x-axis. The higher mean values correspond to a greater influence of features (Bhungeni et al., 2024).

The results show higher mean values for green vegetation classes, such as cropland, grassland, *S. plumosum*, shrubland, and forest, resulting in positive SHAP values for both years of observation. For the same classes, the best-performing bands for both models are SWIR (bands 6 and 7), band 4 (red), and band 3 (green), which are all significantly important for both models and sensitive to vegetation. As expected, the negative contribution, especially for bare or degraded land and built-up classes, was observed in bands 2 (blue) and 3 (green), but increased for BSI; however, NDWI and NDVI proved to be the most important feature contributors, especially for vegetation classes.

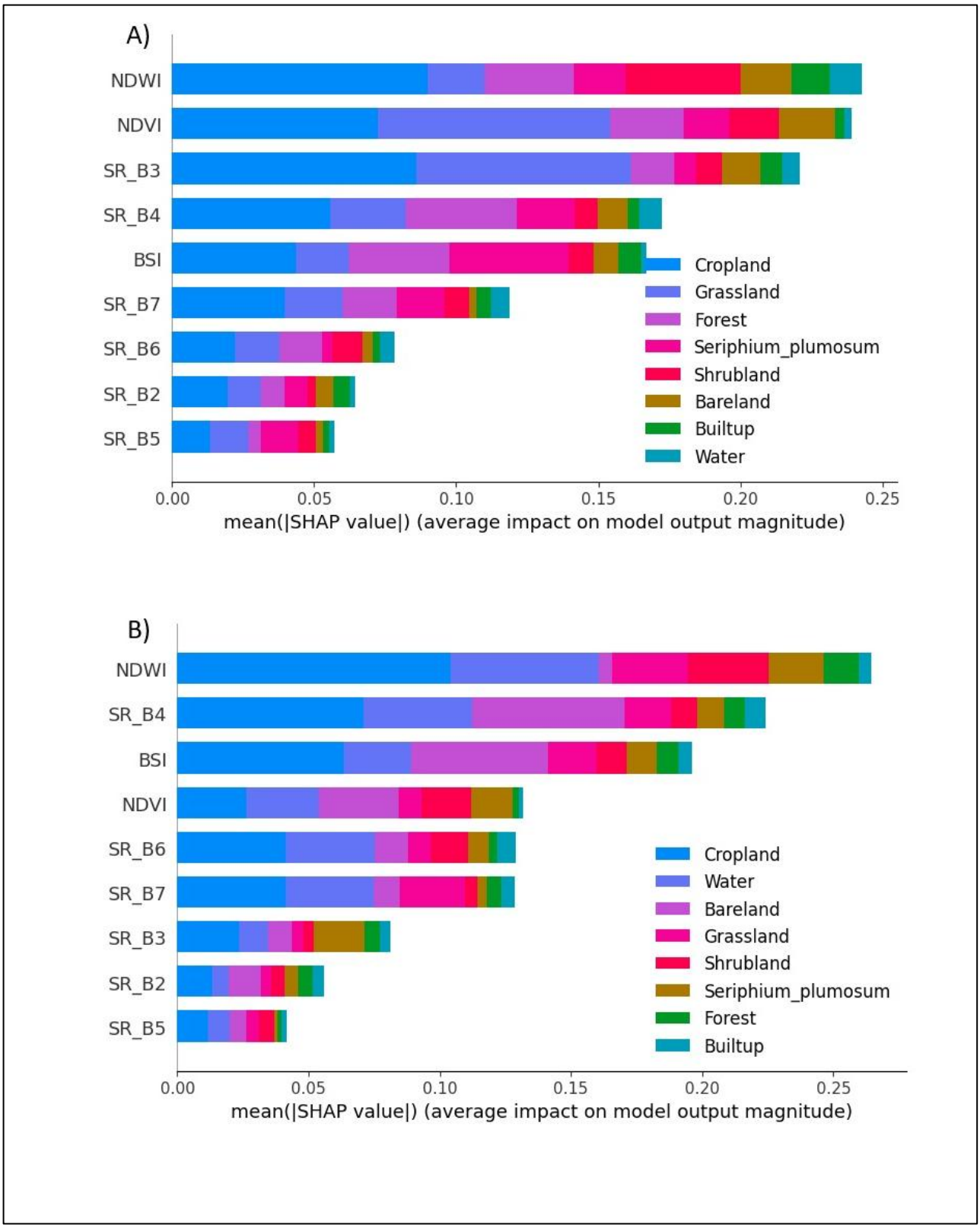


Figure 8: A) mean SHAP values for the 2014 RF model and B) is for the 2024 RF model.

4.5. Maximum Entropy model performance validation

4.5.1. Accuracy assessment

The performance of the Maximum Entropy (MaxEnt) model is confirmed by its sensitivity and specificity (Figure 9A) and the omission graph (Figure 9B), which validate its accuracy (Philips et al., 2006). Both plots are depicted in Figures 9A and 9B. The red line indicates the AUC for the training data, while the blue line shows the AUC for the test data.

The omission rate on test samples was relatively close to the predicted omission rate, and the difference between the two was insignificant. The omission rate on test samples is relatively close to the predicted omission rate, with an insignificant difference (Figure 9B). Both lines are above 0.08 which is above the benchmark for strong model agreement. This indicates that the accepted model is overfitting for the accurate prediction of presence, as confirmed by a close relationship between the prediction results and the presence data.

The study achieved AUC values of 0.956 for training and 0.949 for testing (Figure 9A). Both values are closer to 1 (dimensionality metric varies between 0 and 1, where AUC <0.7, low accuracy, 0.7-0.9, good accuracy and >0.9, very accurate). These AUC results are good indicators of a well-fitting model, as they explain the spatial distribution of *S. plumosum* and predict the probability of presence under current and future conditions.

Based on the species' true presence (occurrence) variable as a model input, the distribution of probability (Figure 10) of presence indicates that correctly classified and background classified as potential presence are all above 0.80 at a cutoff of 0.5. All misclassified presences are below 0.5 and are classified as unsuitable, indicating that the model correctly predicted areas of suitability for *S. plumosum*.

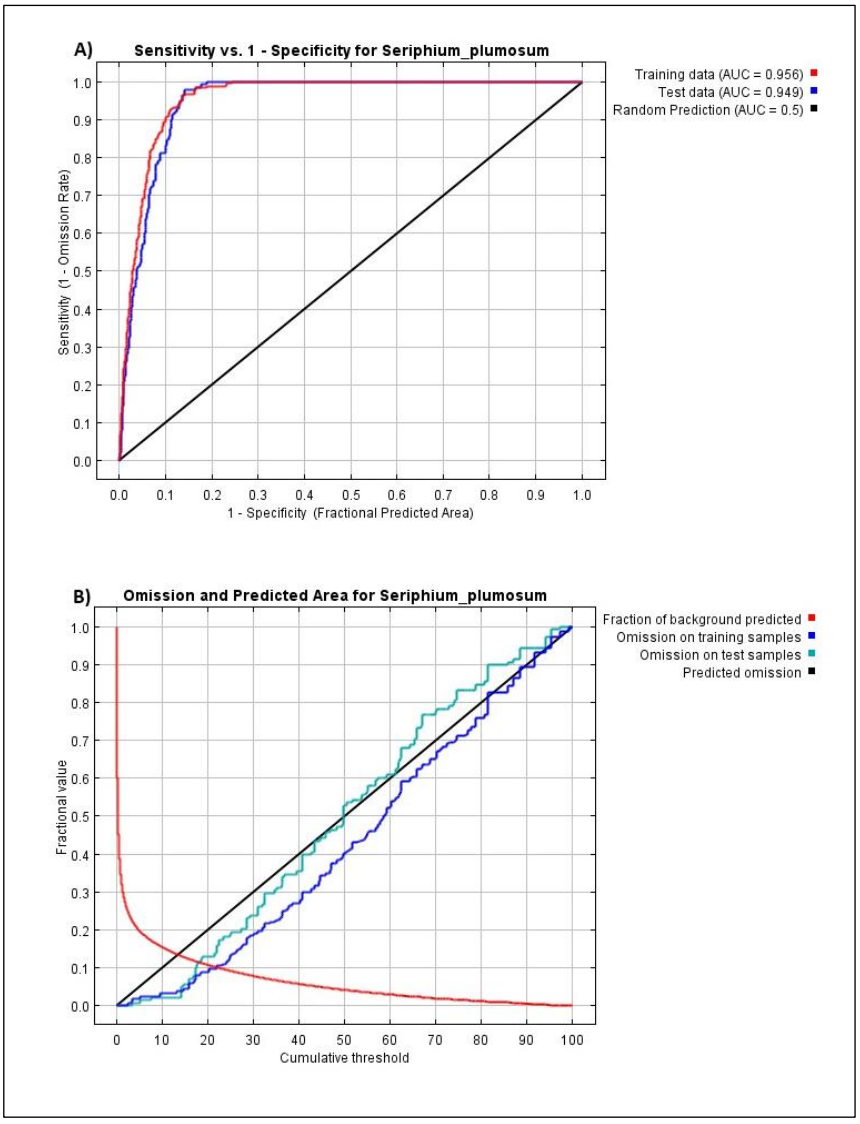


Figure 9: MaxEnt model A) Sensitivity vs Specificity and B) Omission and predicted area for *Seriphium plumosum* prediction.

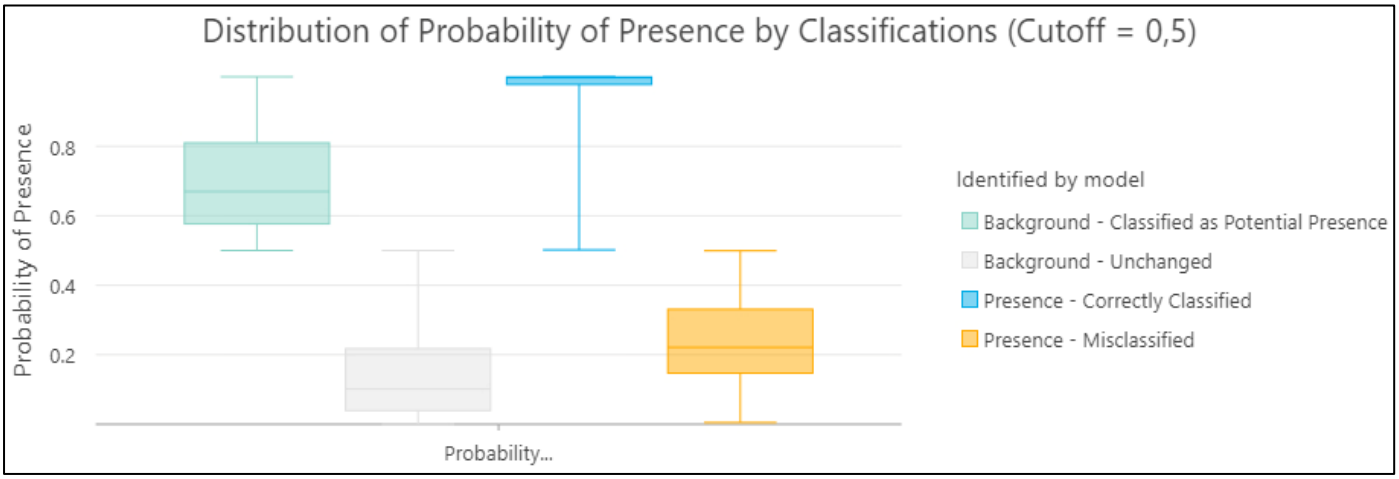


Figure 10: Distribution accuracy of *Seriphium plumosum* species true presence prediction at 0.5 cutoff.

4.5.2. Importance of climatic variables and model preferences

The variable importance of all variables for the model was evaluated by calculating the jackknife for both test gain and training gain for all variables under current and future predicted scenarios (Figure 10). For both tests, the most important variables was TPI (topographic position index), followed by bio-4 (temperature seasonality), and bio-2 (mean diurnal range). They are more significant for the models, as they contribute the largest gain toward acceptable levels of model fit for both the training and test data.

Other variables, for example, slope and elevation, were also important and seem to influence the habitat preference of the *S. plumosum* with AUC values of more than 0.75 as a threshold. In contrast, bio-18 (precipitation of the warmest quarter) and bio-19 (precipitation of the coldest quarter) were the least contributing variables. The two jackknife tests suggest that temperature and precipitation, in concert with topographic variables such as TPI are the most important predictors of the habitat preference and spatial distribution of the *S. plumosum.* The same variables were tested for the future predicted scenario and exhibited the same model output in terms of test and training gain. The majority of variables have an AUC value above 0.8, except for bio-13, bio-14, bio-18, bio-19, and slope, which range between 0.7 and 8.0.

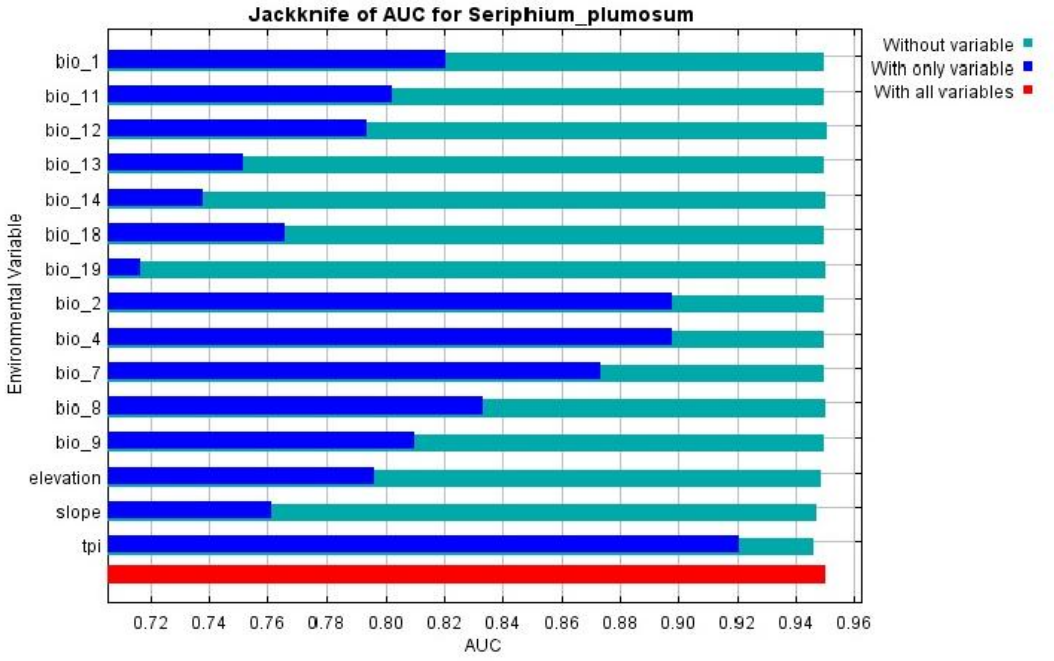


Figure 11: AUC of variables and their importance.

4.6. Contribution and response of predictor variables

Response curves for each variable represent the relationship between habitat suitability and environmental variables. The variables that contain the most information compared to others produced higher gains for the model. Overall, the curves illustrate how the predicted likelihood of presence varies with environmental variables, while all other variables are held constant at their average sample values. For this study, the top two important variables are TPI (with an AUC value of 0.92) and bio-4 (with an AUC value of 0.89), and the bottom two are bio-14 (with an AUC value of 0.75) and bio-19 (with an AUC value of 0.71). Their response curves are shown in Figure 12. For example, sections with low TPI have a high risk of invasion. Infestation is high around a TPI of +20, and a sharp spike increase between +28 and +30 TPI, followed by a gradual decrease in infestation as TPI increases (Figure 12A). Similarly, bio-2 (Figure 12B) shows a sharp increase between 345 and 365 mm. Bio-14 (Figure 11C) and bio-19 (Figure 12D) are both precipitation variables, showing an increase in encroachment as precipitation increases. As expected, the response curves for all variables provided information on the threshold required for a species to thrive or not under varying conditions.

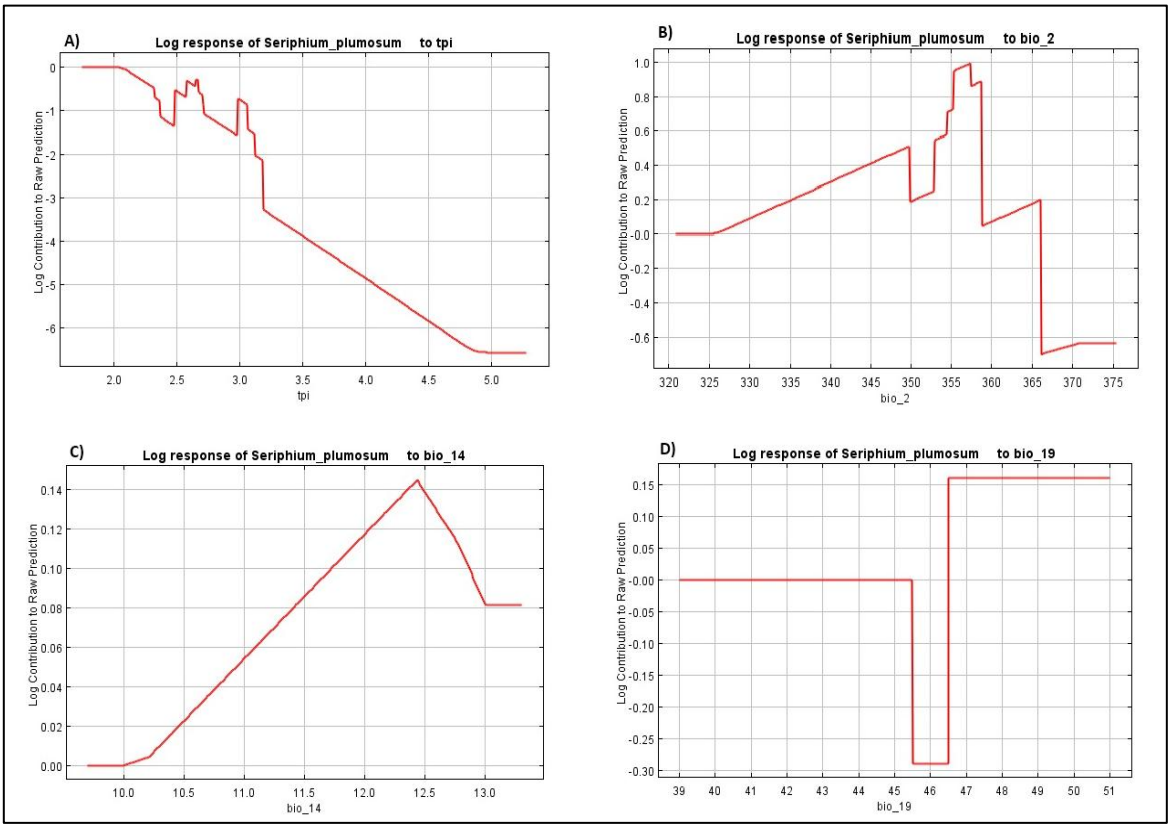


Figure 12: Variable response curves for the top two contributors (TPI and Bio-2) and bottom two contributors (Bio-14 and Bio-19) affecting *Seriphium plumosum* distribution.

4.7. Current and future habitat suitability modelling for *Seriphium plumosum*

The spatial distribution, presented as an output map, was divided into four classes for both the present and future scenarios. The class score or range was categorised as low suitability (0.00-0.25), medium-low suitability (0.25-0.50), medium-high suitability (0.50-0.75), and high suitability (0.75-1.00). Figure 13A shows that the most suitable habitat under current conditions is located in the westernmost part of the study area, characterised by clustered shrubland, with 15.7% high suitability, 3.7% medium-high suitability and 4.2% of medium-low suitability. The easternmost section of the study area is mostly unsuitable. The predicted suitability for future occurrences under the influence of the same bioclimatic and topographic variables is expected to increase, primarily spreading towards the interior, with scattered patches of invasion predicted towards the eastern boundary. There is a noticeable shift of high-intensity infestation from the east to the west. The high-suitability areas are increasing from 15.7% to about 19%, and the medium-high category is increasing from 3.7% to 6.4%. Areas predicted for medium- to low-infestations also increased from 4.2% to 7%. Consequent to the increase in suitability, the unsuitable area has decreased from around 64% to around 55% (Figure 13B).

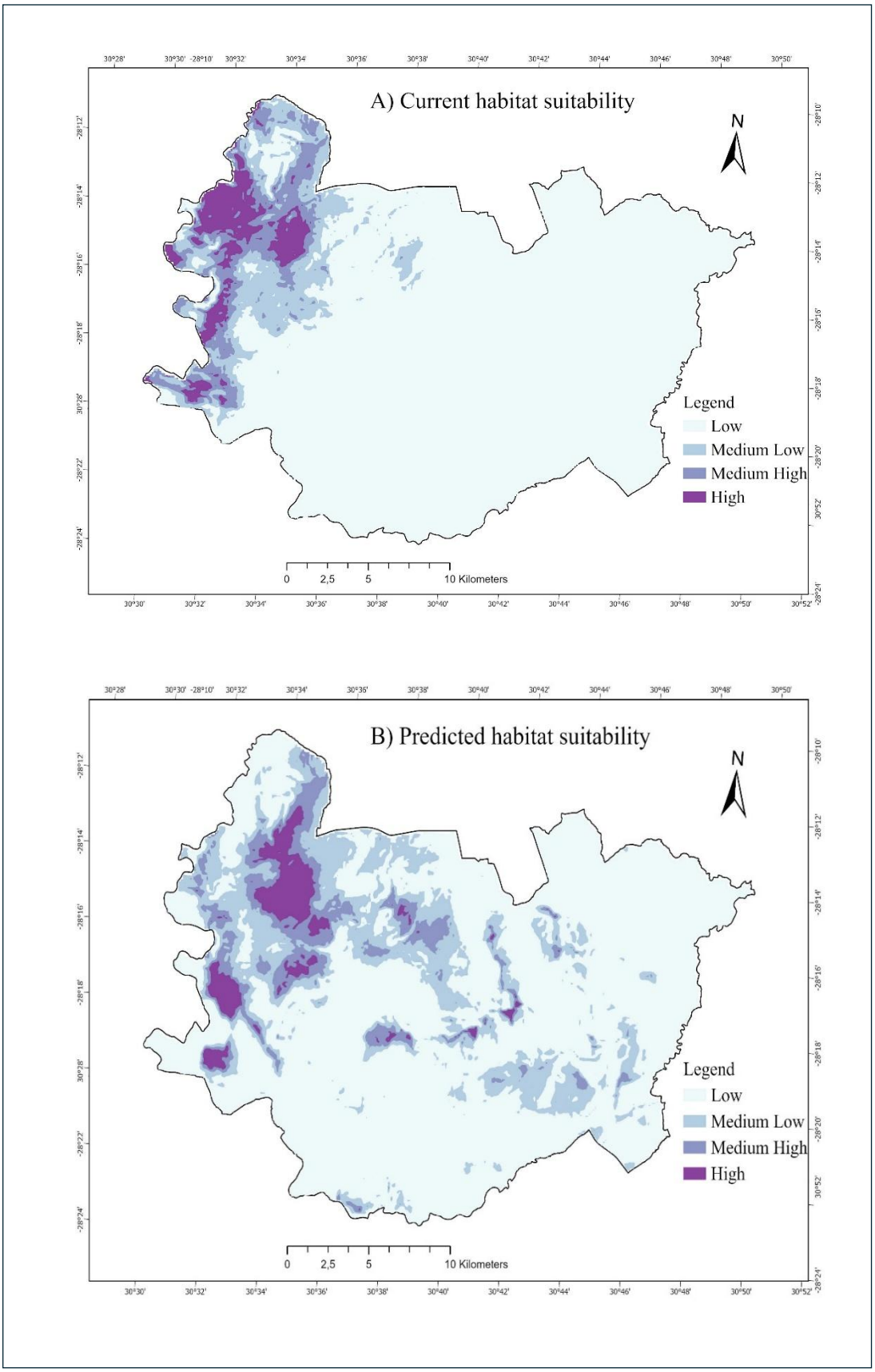


Figure 13: *Seriphium plumosum* habitat suitability maps showing A) current and B) predicted future distribution in the study area located in the Nquthu Municipal area, KwaZulu-Natal, South Africa

CHAPTER FIVE: DISCUSSION

5.1. Introduction

This chapter discusses the study's results by examining factors related to observed changes in land use and land cover classes, the historical, present, and future spatial distribution of S. plumosum, and the perceived threat it poses to rangelands. Furthermore, result that are specific to *S. plumosum* and its associated spatial and temporal variability are discussed. Lastly, the chapter offers concluding remarks that provide specific insights from other studies, highlighting their connections to recommendations suggested by these studies, and suggest future directions and recommendations for related research.

5.2. Random Forest image classification and variable importance

Random Forest achieved high performance accuracy parameters, namely, OA and Kappa coefficient, over 80%, for both years, 2014 and 2024 (Table 7). These results translate to a close match of the map and reality, owing to the high spectral and spatial resolution characteristics of the Landsat-8 image sensor. During the mapping process, Landsat-8 OLI imagery's multispectral bands (visible, NIR, and SWIR) along with spectral indices, namely NDVI, BSI, and NDWI, were used as explanatory variables in the classification process, providing unique spectral information for each class. The NIR, Red and SWIR bands were highly influential. This is due to the water-absorption properties (chlorophyll-sensitive) and the biological characteristics of vegetation (Figures 8A and B). Shortwave infrared bands (SWIR) are influenced by vegetation moisture content and are important for assessing vegetation health and seasonal variations (Hosseiny et al., 2022). The same variable dominance is also confirmed by the study conducted by Dubula et al. (2016), which aimed to discriminate between *S. plumosum* and grass, with the NIR and SWIR regions showing significantly high values. Other bands, such as B5 (Near Infrared), B2 (Blue), and B6 (SWIR 1), decreased in contribution across all classes. The Bare Soil Index (BSI) is high for bare land and built-up areas, indicating the high reflectance of bare surfaces, such as rock, sand, or soil, and significantly contributes to the identification of bare or exposed surfaces.

The contribution of vegetation and soil indices varies significantly between the 2014 and 2024 classifications; for example, NDWI and NDVI were low in the 2014 image compared to the 2024 image. The rainfall data obtained from the South African Weather Services (SAWS) indicates that this is attributable to fluctuations in mean annual rainfall. Many regions in South

Africa experienced a dry cycle between 2014 and 2016, with rainfall falling below 550 mm per year, followed by a record increase of more than 750 mm per year between 2021 and 2024 (South African Weather Services, 2024). The gradual increase in *S. plumosum* encroachment appears to be linked to rainfall fluctuations that also coincide with the study image sample year. Bare land increased in 2024, which indicates that drier conditions between 2014 and 2024 maybe indicative of extensive drought events that may have contributed to the decrease of key vegetation indices (Figures 8A and B). It is, however, worth mentioning that a limitation of this conclusion is the absence of test data to establish this correlation. However, Royimani at al. (2017) also examined the influence of rainfall in a study that monitored the distribution of *Parthenium hysterophoru* L. in Mtubatuba local municipality in KwaZulu-Natal, South Africa and found that there was a strong correlation between annual rainfall and distribution of the species, where the highest infestation recorded correlated with high rainfall means and also declined with decreasing rainfall in the same period. Recently, a study conducted by Jimbo et al. (2023) also confirmed the same bands and indices as highly influential.

Zhao et al. (2024) utilized the NDWI in conjunction with NDVI and Fractional Vegetation Cover (FVC) to develop a comprehensive index that represents the degradation of grasslands and wetlands. Matongera et al. (2017) used NDVI to classify Bracken fern (*Pteridium aquilinum* L) from Landsat-8 combined with Worldview-2 images, which improved classification accuracy from 76.02% to 82.93%–80.08% and 87.8%. Lastly and most recently, Bhungeni et al. (2024) combined NDVI, NDWI, and BSI to aid the classification of different land use and land cover classes in the Umngeni catchment in KwaZulu-Natal using machine learning algorithms. These studies are a testament to the usefulness of spectral indices for vegetation, water, and soil classification studies and pave the way for unending opportunities to improve accuracy indicators for LULC studies, while Mutanga and Skidmore (2004) warn that, for example, NDVI are affected by the saturation problem in high canopy densities. The NDVI has been extensively used to aid the classification of vegetation classes in heterogeneous environments with great success, notably Oumar (2016) for biomass estimation and Matongera et al. (2017) for crop yield studies. Blaschke (2005) highly recommends it for change detection studies as an important supplement to raw spectral bands.

5.3. Spatial variations in Land Use and Land Cover change.

The classification maps revealed that the study area, located within Nquthu Local Municipality in KwaZulu-Natal, South Africa, is primarily dominated by cropland, grassland and *S. plumosum*. Other LULC classes account for a minor share. Variation in spatial extent (Figure 6) shows that, for example, grassland decreased from 15.4% to 8.2% between 2014 and 2024, which is a 7.2% decline. In contrast, *S. plumosum* increased from 3.4% to 12.5% (an increase of 9.1%) in the same period. The dynamics exhibited by these two classes confirm the study and observation by Snyman (2012a), which found that *S. plumosum* outcompeted and displaced grassland cover. This habitat swapping has a negative impact on the grassland ecosystem and agricultural activities, as noted by Hoffman and Vogel (2008). The same results were reported by a study conducted by Nkhwanana et al. (2022), which mapped the encroachment of *S. plumosum* in the Mpumalanga province of South Africa. The study found a 24% loss of grassland cover due to the encroachment of *S. plumosum*. Another study, conducted by Asner (2024) in the Free State province of South Africa, reported that *S. plumosum* encroached on more pastoral agricultural land around 2016 and 2019, and was found to have replaced the grassland cover, where a transition to woody vegetation as a form of bush encroachment has occurred (Mogonong et al., 2024). The observed encroachment by *S. plumosum* into grassland areas poses a significant threat to rangeland functionality and productivity, which are crucial for the survival of livestock and also affect the economic potential of rangelands (Musa et al., 2016). The decline in grass cover, driven by shrub encroachment, reduces herbaceous species diversity, leading to an unbalanced herbivore diet (Kapiyana et al., 2025).

The results of this study further revealed that, although cropland is the dominant land use class, it has decreased over time (62% in 2014 and 57% in 2024). However, this change cannot be attributed solely to *S. plumosum* encroachment, but also to the increase in built-up areas (from 0.8% to 3.7%). The increase in built-up areas has been on an upward trajectory, especially in the rural areas of the KwaZulu-Natal Province, as already reported by Jewett et al. (2015) in their study, which observed changes in land cover between 2005 and 2011. The reported 1.2% increase poses a significant threat to biodiversity, contributing to landscape fragmentation as areas reserved for conservation decline. Another study by Mogonong et al. (2024) in a comparative LULC change detection analysis across three experimental sites in the province of KwaZulu-Natal and Free State in South Africa reported that a decline in cropland was due to households switching from owning and maintaining a large plot of land for agricultural

purposes to a small household garden. The switch is suspected to be primarily due to socio-economic implications related to maintenance costs and persistent extreme climate events. As a consequence, a large portion of land is being abandoned and susceptible to shrub invasion. However, the availability of information quantifying households' garden areas is limited in this study due to Landsat-8's 30 m medium resolution, which limits the mapping of the spatial extent of crop plots per household. The same limitation was reported by Mogonong et al. (2024). Upgrading image data to hyperspectral sensors with at least 3m resolution can be encouraged for such applications to improve these data sets. Urbanisation can also coincide with the conversion of agricultural land into settlement, hence the increase in built-up areas. Ebhuoma et al. (2020) note that a decrease in cropland area is driven by a combination of factors, including political and socio-economic factors, with changes in rainfall and rising temperatures significantly influencing this change. Water bodies such as dams, pans, streams and rivers also decreased by -0.7%, which can be directly linked to increased urbanisation, corresponding to an increased demand for water consumption by livestock and human livelihoods, which has a direct impact on the decrease of surface water (Hoffman & Vogel, 2008). The decrease in water resources is prevalent in South Africa, where water resource yields are in a downward trajectory while demand continues to increase, directly impacting socio-economic growth and development (Ndlovu & Shoko, 2023b). Regrettably, the natural forest also decreased by 3.20% from 5.9% to 2.7% during the same period, along with a 2% decrease in the shrubland class. This decrease in both classes is underscored by the bare land class increasing at an alarming rate of 8.6%, from 4.9% to 13.5%. A similar study conducted by Floreano & De Moraes (2021) in the Rondônia state, Northwest of Brazil in South America, also reported a decline of natural forest areas of about 15.7% between 2009 and 2019 and a further decrease of about 30% is predicted by 2030 due to logging and land converted to settlement as a result of urban development. These changes are depicted in Figures 6 and 7, respectively.

5.4. Bio-climatic variable contribution to model prediction

The *S. plumosum* habitat prediction indicates that temperature-influenced climatic variables such as annual mean temperature (bio-1), mean diurnal range (bio-2), temperature seasonality (bio-4), temperature annual range (bio-7) and mean temperature of wettest quarter (bio-8), in concert with topographic variables, such as elevation, slope, and TPI (Figure 9), are influential drivers of future habitat suitability of *S. plumosum* between 2021 and 2040 period. The MaxEnt

model variable response curves, for example, elevation, show a decrease in distribution with an increase in slope, occupying a wider range at mid- to low-elevation areas. This confirms the reason why dense clusters of distribution are concentrated on gentle or flat surfaces suitable for livestock grazing, where they compete with grassland cover, which affects the grazing potential of the rangeland (Avenant, 2015). The results revealed that as the temperature increases, the soil becomes drier, which enhances the habitat, favouring *S. plumosum* encroachment (Snyman, 2012a). This was also reported in the study conducted by Mengistu et al. (2023), which found that the same bio-climatic variables used in this study also influenced the habitats of different invasive plant species, such as *Prosopis* spp. and *P. glandulosa,* under predicted future climate change scenarios, especially where rainfall and temperatures are projected to increase. Additionally, Adepoju et al. (2020) mapped the encroachment of *S. plumosum* in the Golden Gate Highlands National Park, Free State Province, South Africa, and found that rainfall (0.89 AUC), day temperature (0.83 AUC), and night temperature (0.83 AUC) were highly influential in the encroachment of *S. plumosum*. Similarly, Yan et al. (2024) modelled the spatial distribution of *Alternanthera philoxeroides,* an alien herb species of South American origin, where temperature and precipitation variables exhibited high AUC values above 0.75, with bio-2, which represents the Mean of monthly (max temp – min temp), being the most influential.

The study's primary objective was to quantify the current and historical distribution of *S. plumosum* and to predict future habitat suitability. For the latter purpose, the MaxEnt model was utilised, where different bio-climatic variables were selected as predictors for the model. Accuracy levels of an acceptable model fit were achieved, with an AUC of 0.956 for training and 0.949 for testing, both of which are close to 1. A more accurate prediction range is above the 0.5 cut-off point, classified as potential presence, as shown in Figure 10, which is a good indicator of an acceptable model. The potential presence (ranging from highly suitable to low suitable) under current scenarios reveals that approximately 23.6% of clustered encroachment are predominantly located towards the western boundary, closer to the uMzinyathi River (Figure 13A). At the same time, the remainder, predominantly towards the east, is unsuitable. Furthermore, future suitability is predicted to increase by a total of 10.7% under future climatic scenarios due to predicted climatic variability, indicating a decrease in rainfall and a subsequent increase in drought in many regions of African countries (Hoffman & Vogel, 2009). More invasion is predicted to occur on the interior, extending towards the eastern boundary of the

study site, except in mountainous or high-altitude locations (Figure 13B). The tested bio-climatic predictor variables, as shown in Table 4, suggest that as the temperature increases, the soil will become drier, which will enhance the habitat, favouring *S. plumosum* encroachment. This is confirmed by a study by Snyman (2012), which reported that *S. plumosum* avoids high water soil conditions, such as those found in wetlands with shallow clay soils. This scenario is already unfolding, as confirmed by the 2024 land cover classification results in Figure 5b, which indicate that the distribution of *S. plumosum* is spreading towards the predicted future suitability areas but away from water bodies such as dams and rivers. The current invasion extent confirms the accuracy of the MaxEnt model's habitat suitability predictions. The predicted distribution has the potential to negatively impact ecosystem services and the overall ecological dynamics of the rangeland area (Hoffman & Vogel, 2008), as it will spread to a larger part of the region if no control interventions are implemented.

5.5. Recommendations and limitations

Although this study was conducted on a small scale and was successful, future research could focus on the following: i) test other variables that were not present in this study mainly, topographic derived, for example soil wetness index (SWI) and topographic wetness index (TWI) for predictive analysis of the relationship between habitat and soil water content and, ii) large scale monitoring studies using high spectral image such as Sentinel-2 with red edge band on board sensor and improved Landsat-9 with improved spatial and temporal resolutions are recommended for optimised detection and mapping of invasive plant species (Mutanga & Skidmore, 2007). Although the Landsat-8 image data used in this study bridged the gap between medium and high-spectral-resolution sensors, where possible, hyperspectral sensors such as Worldview-2, QuickBird or UAVs, in combination with more accurate prediction models, are highly recommended to reduce spectral mixing or confusion during classification for optimised detection of invasive plant species (Royimani et al., 2017).

5.6. Conclusion

This study aimed to achieve two things: i) monitor the distribution of *S. plumosum* over ten years from 2014 to 2024 in concert with other LULC thematic classes, and ii) predict its distribution under current and future climate scenarios. Image classification was performed using a random forest algorithm in Google Earth Engine, achieving overall accuracies of 90.1% and 93.5% and Kappa coefficients of 0.84 and 0.87, respectively (Table 5). The importance of

variables across all Landsat-8 OLI multispectral bands was assessed using the SHAP model. The MaxEnt model accurately predicted the presence of *S. plumosum,* as well as its predicted future occurrence, using a combination of selected bioclimatic (temperature- and precipitation-based) and topographic variables. The AUC values of 0.955 for the training data and 0.947 for the test data were achieved using several bioclimatic and topographic variables as predictors for habitat suitability, which proved to influence its distribution. The results indicated that more areas will become suitable for invasion in the coming years (2021-2040) due to changing climatic conditions. The results of this study successfully achieved all its objectives and can therefore serve as the basis for land management policy formulation to enhance biodiversity conservation initiatives.

The need for effective control measures to address rangeland encroachment, which aims to strike a balance between economic sustainability and ecological integrity, is unavoidable. Invasive plant species control mechanisms and management strategies such as those suggested by Kapiyana et al. (2025) that must include, i) limiting further invasion by fencing encroached areas, where possible, to exclude livestock and human access to invaded areas during seed production to limit dispersal opportunities ii) application of strategic mechanical removal of invasive species and bush packing, iii) subsequent reseeding with native grass species such as C4 species to restore grass cover which will also reduce risk of soil erosion can be prioritised. The results achieved by this study provide invaluable information not only to remote sensing studies on land encroachment by weed species but also to ecological studies that seek to understand the interactions between shrub species and how they compete for dominance, as well as the impacts of predicted changing climatic conditions on invasion ecology.

LIST OF REFERENCES

Adepoju, K., Adelabu, S., & Mokubung, C. (2020). Mapping *Seriphium plumosum* encroachment and interaction with wildfire and environmental factors in a protected mountainous grassland. *Environmental Monitoring and Assessment*, *192*(6). https://doi.org/10.1007/s10661-020-08253-x

Angassa, A. and Oba, G. (2008). Effects of management and time on mechanisms of bush encroachment in southern Ethiopia. *African Journal of Ecology*, *46*(2). https://onlinelibrary.wiley.com/doi/abs/10.1111/j.1365-2028.2007.00832.x

Archer, S.D., Widdicombe, C.E., Tarran, G.A., Rees, A.P. and Burkill, P.H. (2001). Production and turnover of particulate dimethylsulphoniopropionate during a coccolithophore bloom in the northern North Sea. *Aquatic Microbial Ecology*, *24*(3), pp.225-24. https://doi.org/10.3354/ame024225

Asner, G. P., Martin, R. E., Carlson, K. M., Rascher, U., & Vitousek, P. M. (2006). Vegetation–Climate Interactions among Native and Invasive Species in Hawaiian Rainforest. *Ecosystems*, *9*(7), 1106–1117. https://doi.org/10.1007/s10021-006-0124-z

Atkinson, D.M., Hung, J.K., Gregory, F.M., Scott, N.A. and Treitz, P.M. (2020). High-Spatial-Resolution Remote Sensing Models for Landscape-Scale CO_2 Exchange in the Canadian Arctic. *Arctic, Antarctic, and Alpine Research*, *52*(1), pp.248-263. https://doi.org/10.1080/15230430.2020.1750805

Avenant P. (2015). Report on the national bankrupt bush (*Seriphium plumosum)* survey (2010-2012). https://doi.org/10.13140/RG.2.2.27655.50088

Avenant P, Riggs I. (2016). Best practices manual for the control and management of. Dep. Agric. For. Fish. 52. Available: https://sasmallholder.co.za/wp-content/uploads/2018/04/Bankrupt-bush-eradication-manual.pdf?utm_source=chatgpt.com

Badenhorst & Reynolds. (2004). PlantAfrica.com website. South African National Biodiversity Institute. Cape Town. Available: https://www.sanbi.org/what-we-do/plantzafrica/

Bayable, G., Cai, J., Mekonnen, M., Legesse, S. A., Ishikawa, K., Imamura, H., & Kuwahara, V. S. (2023). Detection of Water Hyacinth (Eichhornia crassipes) in Lake Tana, Ethiopia, Using Machine Learning Algorithms. *Water*, *15*(5), 880. https://doi.org/10.3390/w15050880

Benavides Rios, E., Sadler, J., Graham, L., & Matthews, T. J. (2024). Species distribution models and island biogeography: Challenges and prospects. In *Global Ecology and Conservation* (Vol. 51, p. e02943). https://doi.org/10.1016/j.gecco.2024.e02943

Bhungeni, O., Ashadevi Ramjatan and Gebreslasie, M. (2024). Evaluating Machine-Learning Algorithms for Mapping LULC of the uMngeni Catchment Area, KwaZulu-Natal. *Remote sensing*, 16(12), pp.2219–2219. https://doi.org/10.3390/rs16122219

Breiman, L. (2001). Random forests. Mach. Learn. 45 (1), 5–32. https://doi.org/10.1023/A:1010933404324

Chen, H., Yang, L., & Wu, Q. (2023b). Enhancing land cover Mapping and Monitoring: an interactive and explainable machine learning approach using Google Earth Engine. *Remote Sensing*, *15*(18), 4585. https://doi.org/10.3390/rs15184585

Clark, D.J., Smithers, J.C., Hughes, D.A., Meier, K.B., Summerton, M.J., Butler, A.J.E. (2009). Design and Development of a Hydrological Decision Support Framework. WRC report No. 1490/1/09: Water Research Commission (WRC), Pretoria, South Africa. Available: https://www.wrc.org.za/wp-content/uploads/mdocs/1490-1-091.pdf

Cord, A. F., Meentemeyer, R. K., Leitão, P. J., & Václavík, T. (2013). Modelling Species Distributions with Remote Sensing Data: Bridging Disciplinary Perspectives. *Journal of Biogeography*, *40*(12), 2226–2227. https://doi.org/10.1111/jbi.12199

Department of Agriculture, Land Reform and Rural Development & Department of Forestry, Fisheries and the Environment, 2024. *Gazetted South African Land Cover Classes and Definitions*. Presented at the National Natural Capital Accounts Forum, July 7, 2024. [online] Available at: [https://www.statssa.gov.za/wp-content/uploads/2024/07/3.-NATIONAL-NCA-FORUM-LANDCOVER-2024-08-07-1.pdf] [Accessed 6 April. 2025].

Dube, T., Shoko, C., Sibanda, M., Madileng, P., Maluleke, X.G., Mokwatedi, V.R., Tibane, L. and Tshebesebe, T. (2020). Remote sensing of invasive Lantana camara (Verbenaceae) in semiarid savanna rangeland ecosystems of South Africa. *Rangeland Ecology & Management*, *73*(3), pp.411-419. https://doi.org/10.1016/j.rama.2020.01.003

Dubula, B., Tefsamichael, S. G., & Rampedi, I. T. (2016). Assessing the potential of remote sensing to discriminate invasive *Seriphium plumosum* from grass. *South African Journal of Geomatics*, *5*(2), 201. https://doi.org/10.4314/sajg.v5i2.8

Ebhuoma, E.E., Donkor, F.K., Ebhuoma, O.O., Leonard, L. & Tantoh, H.B. (2020). Subsistence farmers' differential vulnerability to drought in Mpumalanga province, South Africa: Under the political ecology spotlight. Cogent Social Sciences, **6**, p.1792155. https://doi.org/10.1080/23311886.2020.1792155

Eldridge DJ, Ding J. (2021). Remove or retain: the ecosystem effects of woody encroachment and removal are linked to plant structural and functional traits. New Phytologist. 229: 2637 – 2646. https://doi.org/10.1111/nph.17045

Everitt, J. H., and Deloach, C. J. (1990). Remote Sensing of Chinese Tamarisk (*Tamarix chinensis*) and Associated Vegetation. *Weed Science*, 38, pp. 273-278. https://doi.org/10.1017/S0043174500056526

FAO. (2008). Livestock policy and poverty reduction. Rome, Italy: Food and Agriculture Organisation. Livestock policy brief 04. 8 p. Available at: ftp://ftp.fao.org/docrep/fao/010/i0265e/i0265e00.pdf. Accessed 16 April 2024.

FAO. (2011). World Census of Agriculture: analysis and international comparison of the results (1996-2005). FAO Statistical Development Series No. 13. (Columns 3 and 4). Rome. https://www.fao.org/3/i2680e/i2680e.pdf

Fernández, A.J., Molero, F., Becerril-Valle, M., Coz, E., Salvador, P., Artíñano, B. and Pujadas, M. (2018). Application of remote sensing techniques to study aerosol water vapour uptake in a real atmosphere. *Atmospheric Research*, *202*, pp.112-127. https://doi.org/10.1016/j.atmosres.2017.11.020

Freeman, D., Garety, P.A., Kuipers, E., Fowler, D. and Bebbington, P.E. (2002). A cognitive model of persecutory delusions. *British Journal of Clinical Psychology*, *41*(4), pp.331-347. https://doi.org/10.1348/014466502760387461

Feng, S. and Fu, Q. (2013). Expansion of global drylands under a warming climate. *Atmospheric Chemistry and Physics*, *13*(19), pp.10081-10094. 10.5194/acp-13-10081-2013

Floreano, I.X. and de Moraes, L.A.F. (2021). Land use/land cover (LULC) analysis (2009–2019) with Google Earth Engine and 2030 prediction using Markov-CA in the Rondônia State, Brazil. *Environmental Monitoring and Assessment*, 193(4), p.239. Available at: https://doi.org/10.1007/s10661-021-09016-y.

Fick, S.E. and Hijmans, R.J. (2017). WorldClim 2: new 1 km spatial resolution climate surfaces for global land areas. International Journal of Climatology, 37(12), pp.4302. https://doi.org/10.1002/joc.5086

Forsyth, A.T., Gibson, L.A. and Turner, A.A. (2014). Assessment of SPOT 6 imagery for mapping the invasive alien plant species Pinus spp. in a mountainous area of the Western Cape. In *Proceedings of the Second AfricaGEO Conference* (pp. 1-12).

Fourcade, Y., Engler, J.O., Rödder, D. and Secondi, J. (2014). Mapping species distributions

with MAXENT using a geographically biased sample of presence data: a performance assessment of methods for correcting sampling bias. *PloS one*, *9*(5), p.e97122. https://journals.plos.org/plosone/article?id=10.1371/journal.pone.0097122

Gemedo-Dalle, Maass, B.L. and Isselstein, J. (2006). Rangeland condition and trend in the semi-arid Borana lowlands, southern Oromia, Ethiopia. *African Journal of Range and Forage Science*, *23*(1), pp.49-58. https://doi/abs/10.2989/10220110609485886

Gross, G., Helder, D., Begeman, C., Leigh, L., Kaewmanee, M. and Shah, R. (2022). Initial cross-calibration of Landsat 8 and Landsat 9 using the simultaneous underfly event. *Remote Sensing*, 14(10), p.2418. https://doi:10.3390/rs14102418

Hoffman, T., & Vogel, C. (2008). Climate Change Impacts on African Rangelands. Rangelands, 30(3), 12-17. https://www.jstor.org/stable/10.2111/1551-501X(2008)30[12:CCIOAR]2.0.CO;2

Jama, B. and Zeila, A. (2005). Agroforestry in the drylands of eastern Africa: a call to action. ICRAF Working Paper – No. 1. Nairobi: World Agroforestry Centre. Available: *https://www.cifor-icraf.org/publications/downloads/Publications/PDFS/wp05043.pdf*?

Jewitt, D., Goodman, P.S., Erasmus, B.F.N., O'Connor, T.G. & Witkowski, E.T.F. (2015) Systematic land-cover change in KwaZulu-Natal, South Africa: Implications for biodiversity. *South African Journal of Science*, 111(9/10), pp. 1–9. https://doi.org/10.17159/sajs.2015/20150019

Kapiyana, B. C., Mndela, M., & Thamaga, H. K. (2025). Shrub invasion drives herbaceous vegetation degradation in semi-arid rangelands of the Eastern Cape Province of South Africa. *South African Journal of Botany, 185,* 41–52. https://doi.org/10.1016/j.sajb.2025.07.034

Kaur, H., Tyagi, S., Mehta, M. and Singh, D. (2023). Time series (2001/2002–2021) analysis of Earth observation data using Google Earth Engine (GEE) for detecting changes in land use land cover (LULC) with specific reference to forest cover in East Godavari Region, Andhra Pradesh, India. *Journal of Earth System Science*, *132*(2), p.86. https://doi.org/10.1007/s12040-023-02099-w

Kishore, B.S.P.C., Kumar, A. and Saikia, P. (2024). Mapping forest phenological shift in Nilgiri Biosphere Reserve, Western Ghats: Response to climate change. *Remote Sensing Applications: Society and Environment*, *36*, p.101325. https://doi.org/10.1016/j.rsase.2024.101325

Koekemoer, M. (2001). Systematics of the *Metalasia* group in the Relhaniinae (Gnaphalieae – Asteraceae). PhD thesis, Rand Afrikaans University, South Africa.

Hosseiny, B., Abdi, A. M., & Jamali, S. (2022). Urban land use and land cover classification with interpretable machine learning – A case study using Sentinel-2 and auxiliary data. *Remote Sensing Applications Society and Environment*, *28*, 100843. https://doi.org/10.1016/j.rsase.2022.100843

Huang, C. Y., & Asner, G. P. (2009). Applications of Remote Sensing to Alien Invasive Plant Studies. *Sensors*, *9*(6), 4869–4889. https://doi.org/10.3390/s90604869

Jewitt, D., Goodman, P.S., Erasmus, B.F.N., O'Connor, T.G. and Witkowski, E.T.F. (2015). Systematic land-cover change in KwaZulu-Natal, South Africa: Implications for biodiversity. *South African Journal of Science*, 111(9/10), Art. #2015-0019, 9 pages. Available at: http://dx.doi.org/10.17159/sajs.2015/20150019.

Jombo, S. and Adelabu, S.A. (2023). Evaluating Landsat-8, Landsat-9 and Sentinel-2 imageries in land use and land cover (LULC) classification in a heterogeneous urban area. *GeoJournal.* https://doi.org/10.1007/s10708-023-10982-8

Jordaan, D. (2009)**.** Bankruptbush (Slangbos)—A silent threat to grasslands*?* Grassroots Newsletter, Grassland Society of Southern Africa, 9, pp.40–42.

Joshi, C., De Leeuw, J., Skidmore, A.K., Van Duren, I.C. and Van Oosten, H. (2006). Remotely sensed estimation of forest canopy density: A comparison of the performance of four methods. *International Journal of Applied Earth Observation and Geoinformation*, *8*(2), pp.84-95. https://doi.org/10.1016/j.jag.2005.08.004

Ju, J., Gopal, S. & Kolaczyk, E.D. (2005) On the Choice of Spatial and Categorical Scale in Remote Sensing Land Cover Classification. *Remote sensing of Environment*, 96 pg. 62 – 77 https://doi.org/10.1016/j.rse.2005.01.016

Juliá, R., Holland, D. W., & Guenthner, J. (2007). Assessing the economic impact of invasive species: The case of yellow starthistle (*Centaurea solstitialis L.*) in the rangelands of Idaho, USA. *Journal of Environmental Management*, *85*(4), 876–882. https://doi.org/10.1016/j.jenvman.2006.10.024

Kaur, H.; Tyagi, S.; Mehta, M.; Singh, D. (2023).Time Series (2001/2002–2021). Analysis of Earth Observation Data Using Google Earth Engine (GEE) for Detecting Changes in Land Use Land Cover (LULC) with Specific Reference to Forest Cover in East Godavari Region, Andhra Pradesh, India. J. Earth Syst. Sci. 2023, 132, 86. https://doi.org/10.1007/s12040-023-02099-w

Kishore, B. S. P. C., Kumar, A., Saikia, P., Lele, N., Srivastava, P., Pulla, S., Suresh, H., Bhattarcharya, B. K., Khan, M. L., & Sukumar, R. (2024). Mapping of under storey invasive plant species clusters of *Lantana camara* and *Chromolaena odorata* using airborne hyperspectral remote sensing. *Advances in Space Research*, *73*(2), 1379–1396. https://doi.org/10.1016/j.asr.2022.12.026

Landgrebe, D.A., (1999). Some fundamentals and methods for hyperspectral image data analysis. In *Systems and technologies for clinical diagnostics and drug discovery II* (Vol. 3603, pp. 104-113). SPIE. https://doi.org/10.1117/12.355800

Lass, L.W., Prather, T.S., Glenn, N.F., Weber, K.T., Mundt, J.T. and Pettingill, J. (2005). A review of remote sensing of invasive weeds and example of the early detection of spotted knapweed (Centaurea maculosa) and babys breath (*Gypsophila paniculata*) with a hyperspectral sensor. *Weed Science*, *53*(2), pp.242-251. https://doi.org/10.1614/WS-04-044R2

Lillesand, T.M., Kiefer, R.W. &Chipman, J.W. (2004) *Remote Sensing and Image Interpretation (5th Ed.)*. New York, John Wiley and Sons, Inc. ISBN-13: 978-0471152279

Lu, D. and Weng, Q. (2007). A survey of image classification methods and techniques for improving classification performance. *International journal of Remote sensing*, *28*(5), pp.823-870. https://doi.org/10.1080/01431160600746456

Ludwig A, Meyer, H., and Nauss, T. (2016.) Automatic classification of Google Earth images for a larger-scale monitoring of bush encroachment in South Africa. International Journal of Applied Earth Observation and Geoinformation 50 (2016)89–94. https://doi.org/10.1016/j.jag.2016.02.005

Lundberg, S.M. and Lee, S.I. (2017). A unified approach to interpreting model predictions. *Advances in Neural Information Processing Systems*, *30*. https://doi.org/10.5555/3295222.3295230

Madonsela, S., Cho, M. A., Mathieu, R., Mutanga, O., Ramoelo, A., Kaszta, A., Van De Kerchove, R., & Wolff, E. (2017). Multi-phenology WorldView-2 imagery improves remote sensing of savannah tree species. *International Journal of Applied Earth Observation and Geoinformation*, *58*, 65–73. https://doi.org/10.1016/j.jag.2017.01.018

Mashala, M.J., Dube, T., Ayisi, K.K. and Ramudzuli, M.R., (2023). Using the Google Earth Engine cloud-computing platform to assess the long-term spatial-temporal dynamics of land use and land cover within the Letaba watershed, South Africa. *Geocarto International*, *38*(1), p.2252781. https://doi.org/10.1080/10106049.2023.2252781

Mananze, S., Pôças, I. and Cunha, M. (2020). Mapping and assessing the dynamics of shifting

agricultural landscapes using Google Earth Engine cloud computing, a case study in Mozambique. *Remote Sensing*, *12*(8), p.1279. https://doi.org/10.3390/rs12081279

Mantero, P., Moser, G., Serpico, S.B. (2005). Partially supervised classification of remote sensing images through SVM-based probability density estimation. IEEE Transactions on Geoscience and Remote Sensing, 43(3), 559–570. https://doi.org/10.1109/TGRS.2004.842022

Maphanga, T., Dube, T., Shoko, C., & Sibanda, M. (2022). Advancements in the satellite sensing of the impacts of climate and variability on bush encroachment in savannah rangelands. *Remote Sensing Applications*, *25*, 100689. https://doi.org/10.1016/j.rsase.2021.100689.

Masek, J. G., Wulder, M. A., Markham, B., Mccorkel, J., Crawford,C. J., Storey, J., & Jenstrom, D. T. (2020). Landsat 9: Empowering open science and applications through continuity. *Remote Sensing of Environment, 248*, 111968. https://doi.org/10.1016/j.rse.2020.111968

Masemola, C., Cho, M. A., & Ramoelo, A. (2020). Sentinel-2 time series-based optimal features and time window for mapping invasive Australian native Acacia species in KwaZulu-Natal, South Africa. *International Journal of Applied Earth Observation and Geoinformation*, *93*, 102207. https://doi.org/10.1016/j.jag.2020.102207

McFeeters, S.K. (1996). The use of the Normalized Difference Water Index (NDWI) in the delineation of open water features. *International Journal of Remote Sensing*, 17(7), pp.1425–1432**.** https://doi.org/10.1080/01431169608948714

Mather, P.M. and Koch, M. (2022). *Computer processing of remotely sensed images*. John Wiley & Sons. ISBN-13: 978–1119502821.

Matongera, T.N., Mutanga, O., Dube, T. and Sibanda, M. (2017). Detection and mapping the spatial distribution of bracken fern weeds using the Landsat 8 OLI new generation sensor. *International Journal of Applied Earth Observation and Geoinformation*, *57*, pp.93-103. https://doi.org/10.1016/j.jag.2016.12.006

McCarty, D. A., Kim, H. W., & Lee, H. K. (2020). Evaluation of the light gradient boosted machine learning technique in large-scale land use and land cover classification. *Environments*, *7*(10), 84. https://doi.org/10.3390/environments7100084

McCord, S.E., Brehm, J.R., Burnett, S.H., Dietrich, C., Edwards, B., Metz, L.J., Narvaez, M.H., Pierson, F., Ramirez, K.S., Stauffer, N.G. and Webb, N.P. (2022). A framework and toolset for standardizing agroecosystem indicators. *Ecological Indicators*, *144*, p.109511. https://doi.org/10.1016/j.ecolind.2022.109511

Mean Annual Rainfall Data. (n.d.). South African Weather Services. Retrieved June 1, 2025, from https://www.weathersa.co.za/home/historicalrain.

Mengistu, A. G., Tesfuhuney, W. A., Woyessa, Y. E., & Steyn, A. S. (2023). Potential distribution of selected invasive alien plants under current and future climate change scenarios in South Africa. *Heliyon*, *9*(9), e19867. https://doi.org/10.1016/j.heliyon.2023.e19867.

Michez, A., Piégay, H., Jonathan, L., Claessens, H., & Lejeune, P. (2016). Mapping of riparian invasive species with supervised classification of Unmanned Aerial System (UAS) imagery. *International Journal of Applied Earth Observation and Geoinformation*, *44*, 88–94. https://doi.org/10.1016/j.jag.2015.06.014.

Mogonong, B. P., Twine, W., Feig, G. T., Van der Merwe, H. & Fisher, J. T. (2024). 'Influences of climate variability on land use and land cover change in rural South Africa', *Remote Sensing*, 16(7), article 1200. https://doi.org/10.3390/rs16071200.

Mokoka, T. A., O'Connor, T. G., & Jary, D. (2016). Ecology and spread of *Seriphium plumosum* in South African grasslands. *South African Journal of Botany***,** 104, 45–52

Moore, A. and Van Niekerk,J.P. (1987). Bosindringing in die Vrystaatstreek: Indringerspesies

en die omvangvan die problem. Dept van Landbou en watervoorsiening. Glen Agric. 16:1.

Mtyobila, V. E., & Shoko, C. (2024). Modelling lantana camara invasion in the Inkomati catchment in Mpumalanga, South Africa. *Physics and Chemistry of the Earth Parts a/B/C*, *135*, 103633. https://doi.org/10.1016/j.pce.2024.103633

Müllerová, J., Brůna, J., Bartaloš, T., Dvořák, P., Vítková, M. and Pyšek, P. (2017). Timing is important: Unmanned aircraft vs. satellite imagery in plant invasion monitoring. *Frontiers in Plant Science*, *8*, p.887. https://doi.org/10.3389/fpls.2017.00887

Munyati, C. and Makgale, D. (2009) 'Multitemporal Landsat TM imagery analysis for mapping and quantifying degraded rangeland in the Bahurutshe communal grazing lands, South Africa', *International Journal of Remote Sensing*, 30(14), pp. 3649–3668. https://doi.org/10.1080/01431160802592534.

Mutanga, O., & Skidmore, A. K. (2004). Hyperspectral band depth analysis for a better estimation of grass biomass (Cenchrus ciliaris) measured under controlled laboratory conditions. *International Journal of Applied Earth Observation and Geoinformation*, *5*(2), 87–96. https://doi.org/10.1016/j.jag.2004.01.001.

Musa, M., Hakim Hashim, & Mukeram Teha. (2016). Rangeland degradation: Extent, impacts, and Alternative Restoration techniques in the Rangelands of Ethiopia. In *Tropical and Subtropical Agroecosystems* (Vol. 19, pp. 305–318). https://doi.org/10.56369/tsaes.2234

Namugize, J. N., Jewitt, G., & Graham, M. (2018). Effects of land use and land cover changes on water quality in the uMngeni river catchment, South Africa. *Physics and Chemistry of the Earth Parts a/B/C*, *105*, 247–264. https://doi.org/10.1016/j.pce.2018.03.013.

Nath, B., Niu, Z. and Mitra, A.K. (2019). Observation of short-term variations in the clay minerals ratio after the 2015 Chile great earthquake (8.3 Mw) using Landsat 8 OLI data. *Journal of Earth System Science*, *128*(5), p.117. https://doi.org/10.1007/s12040-019-1129-2

NASA Landsat Science, no date. *Operational Land Imager (OLI) Requirements and Design*. [online] Available at: https://landsat.gsfc.nasa.gov/satellites/landsat-8/spacecraft-instruments/operational-land-imager/oli-requirements [Accessed 6 Aug. 2025].

Ndlovu, H., & Shoko, C. (2023a). Assessing Lantana camara spatial distribution in response to rainfall and temperature variations in the Inkomati catchment in Mpumalanga. *Physics and Chemistry of the Earth Parts a/B/C*, *132*, 103470. https://doi.org/10.1016/j.pce.2023.103470.

Ngarega, B. K., Masocha, V. F., & Schneider, H. (2021a). Forecasting the effects of bioclimatic characteristics and climate change on the potential distribution of *Colophospermum mopane* in southern Africa using Maximum Entropy (Maxent). *Ecological Informatics*, *65*, 101419. https://doi.org/10.1016/j.ecoinf.2021.101419.

Nkhwanana, N., Adam, E., & Ramoelo, A. (2022b). Assessing the utility of Sentinel-2 MSI in mapping an encroaching *Serephium plumosum* in South African rangeland. *Applied Geomatics*, *14*(3), 435–449. https://doi.org/10.1007/s12518-022-00423-5.

Nigatu, L., Hassen, A., Sharma, J. and Adkins, S.W. (2010). Impact of *Parthenium hysterophorus* on grazing land communities in north-eastern Ethiopia. *Weed Biology and Management*, *10*(3), pp.143-152. https://doi.org/10.1111/j.1445-6664.2010.00378.x

Ngubane, Z., Odindi, J., Mutanga, O. and Slotow, R. (2014). Assessment of the contribution of WorldView-2 strategically positioned bands in Bracken fern (Pteridium aquilinum (L.) Kuhn) mapping. *South African Journal of Geomatics*, *3*(2), pp.210-223. Available: https://www.sajg.org.za/index.php/sajg/article/view/203

Nowak, M.M., Dziób, K. and Bogawski, P. (2018). Unmanned Aerial Vehicles (UAVs) in environmental biology: A review. *European Journal of Ecology*, *4*(2), pp.56-74. https://doi.org/10.2478/eje-2018-0012

Odindi, J.O., Bangamwabo, V. and Mutanga, O. (2015). Assessing the Value o f Urban Green spaces in Mitigating Multi-Seasonal Urban heat using MODISL and Surface Temperature (LST) and Landsat 8 data. *International Journal of Environmental Research*, *9*(1), pp.9-18. https://doi.org/10.22059/ijer.2015.868

Orieschnig, C. A., Belaud, G., Venot, J.-P., Massuel, S., and Ogilvie, A. (2021). Input imagery, classifiers, and cloud computing: Insights from multi-temporal LULC mapping in the Cambodian Mekong Delta. *European Journal of Remote Sensing*, *54*(1), 398–416. https://doi.org/10.1080/22797254.2021.1948356.

Oumar, Z. (2016). Assessing the utility of the SPOT 6 sensor in detecting and mapping Lantana camera for a community clearing project in KwaZulu-Natal, South Africa. *South African Journal of Geomatics*, *5*(2), 214. https://doi.org/10.4314/sajg.v5i2.9.

Peerbhay, K., Mutanga, O., Lottering, R. and Ismail, R. (2016). Mapping *Solanum mauritianum* plant invasions using WorldView-2 imagery and unsupervised random forests. *Remote Sensing of Environment*, 182, pp.39–48. https://doi.org/10.1016/j.rse.2016.04.025.

Phillips, S.J., Anderson, R.P. and Schapire, R.E. (2006). Maximum entropy modelling of species geographic distributions. *Ecological modelling*, *190*(3-4), pp.231-259. https://doi.org/10.1016/j.ecolmodel.2005.03.026

Pule, H. T., Tjelele, J. T., Hattas, D., & Tedder, M. J. (2023). Evaluating the Potential Use of *Seriphium plumosum* L. as Forage in the Semiarid Grassland of Gauteng Province, South Africa. *Rangeland Ecology & Management*, *87*, 30–33. https://doi.org/10.1016/j.rama.2022.11.007

Purkis, S.J. and V Klemas. (2011). *Remote sensing and global environmental change*. Chichester, West Sussex, Uk ; Hoboken, N.J.: Wiley-Blackwell. ISBN: 9781444339352. https://doi.org/10.1002/9781118687659

Ramoelo, A., Stolter, C., Joubert, D., Cho, M.A., Groengroeft, A., Madibela, O.R., Zimmermann, I. and Pringle, H. (2018). Rangeland monitoring and assessment: a review. https://doi.org/10.7809/b-e.00320

Retkute, R., Crew, K.S., Thomas, J.E. and Gilligan, C.A. (2025). Detection of banana diseases based on Landsat-8 data and machine learning. *Remote Sensing*, 17(13), p.2308. Available at: https://doi.org/10.3390/rs17132308.

Reynolds, J.F., Smith, D.M.S., Lambin, E.F., Turner, B.L., Mortimore, M., Batterbury, S.P., Downing, T.E., Dowlatabadi, H., Fernández, R.J., Herrick, J.E. and Huber-Sannwald, E., (2007). Global desertification: building a science for dryland development. *science*, *316*(5826), pp.847-851. https://doi.org/10.1126/science.1131634

Rikimaru, A., Roy, P.S. & Miyatake, S., (2002). Tropical forest cover density mapping. Tropical Ecology, 43(1), pp.39–47.

Rios, E., (2024). Using neural networks for image analysis in general physiology. *Journal of General Physiology*, *156*(10), p.e202413623. https://doi.org/10.1085/jgp.202413623

Rouse, J.W., Haas, R.H., Schell, J.A. & Deering, D.W., (1974). Monitoring vegetation systems in the Great Plains with ERTS. In: *Third Earth Resources Technology Satellite-1 Symposium. Volume I: Technical Presentations*, NASA SP-351, pp. 309–317. NASA, Washington, D.C. https://ntrs.nasa.gov/citations/19740022614?utm_source=chatgpt.com

Royimani, L., (2017). Spatial-temporal mapping of Parthenium (P. Hysterophorum) in the Mtubatuba municipality, KwaZulu-Natal, South Africa. School of Agricultural, Earth and Environmental Sciences, University of KwaZulu-Natal. Available: https://ukzn-dspace.ukzn.ac.za/bitstreams/041162dc-1535-4c61-bff9-56e7a1d52a40/download

Royimani, L., Mutanga, O., Odindi, J., Dube, T., & Matongera, T. N., (2019). Advancements in satellite remote sensing for mapping and monitoring of alien invasive plant species (AIPs). *Physics and Chemistry of the Earth/Physics and Chemistry of the Earth. Parts a/B/C*, *112*, 237–245. https://doi.org/10.1016/j.pce.2018.12.004 .

Rutherford, M.C.; Mucina, L. (2006). The Vegetation of South Africa, Lesotho and Swaziland. Strelitzia 19; South African Biodiversity Institute: Pretoria, South Africa; 816p. https://www.sanbi.org/wp-content/uploads/2018/05/Strelitzia-19.pdf

Shabani, F., Kalantar, B. and Esmaeili, A. (2020). Invasive weed species' threats to global biodiversity: Future scenarios of changes in the number of invasive species in a changing climate. *Ecological Indicators*, 116, p.106436. Available at: https://doi.org/10.1016/j.ecolind.2020.106436.

Shoko, C. and Mutanga, O. (2017). Examining the strength of the newly-launched Sentinel 2 MSI sensor in detecting and discriminating subtle differences between C3 and C4 grass species. *ISPRS journal of photogrammetry and remote sensing*, *129*, pp.32-40. https://doi.org/10.1016/j.isprsjprs.2017.04.010

Schmidt E, Lotter M, McCleland W. (2002). Tree and shrubs of the Mpumalanga and Kruger National Park: Jacaranda Media Publisher, Pretoria. ISBN-13: 978-1-919777-30-6

Singini, E. J., McMillan, B. M., Newete, S. W., & Witkowski, E. T. (2024). Ecological drivers of *Seriphium plumosum* encroachment: Implications for management and conservation. *South African Journal of Botany, 176*, 21–28. https://doi.org/10.1016/j.sajb.2024.11.001

Snyman HA. (2009) Germination potential of *Seriphium plumosum* (bankrupt bush, slangbos or vaalbos). Grassroots Newsl. Grassland Society of South Africa. 9, 6. https://grassland.org.za/sites/default/files/2023-11/February%202009.pdf?

Snyman, H.A. (2010). Knowledge of seed ecology essential for *Seriphium plumosum* control. Grassroots: publication of the Grassland Society of Southern Africa. Vol. 10 (1). p. 9-14. https://grassland.org.za/sites/default/files/2023-11/February%202010.pdf

Snyman, H.A. (2012a). Control measures for the encroacher shrub *Seriphium plumosum*, South African Journal of Plant and Soil, 29:3-4, 157-163, https://doi.org/10.1080/02571862.2012.745905.

Snyman, H. (2012). Habitat preferences of the encroacher shrub, *Seriphium plumosum*. *South African Journal of Botany*, *81*, 34–39. https://doi.org/10.1016/j.sajb.2012.05.001

Somers, B. and Asner, G.P. (2013). Multi-temporal hyperspectral mixture analysis and feature selection for invasive species mapping in rainforests. *Remote Sensing of Environment*, *136*, pp.14-27. https://doi.org/10.1016/j.rse.2013.04.015

Steven J. Phillips, Miroslav Dudík, Robert E. Schapire. [Internet] Maxent software for modelling species niches and distributions (Version 3.4.1). Available from url: http://biodiversityinformatics.amnh.org/open_source/maxent/. Accessed on 2025-3-3.

Strand, E.K., Smith, A.M., Bunting, S.C., Vierling, L.A., Hann, D.B. and Gessler, P.E. (2006). Wavelet estimation of plant spatial patterns in multitemporal aerial photography. *International Journal of Remote Sensing*, *27*(10), pp.2049-2054. https://doi.org/10.1080/01431160500444764

Underwood, E., Ustin, S. & DiPietro, D. (2003). *Mapping nonnative plants using hyperspectral imagery.* Remote Sensing of Environment, 86, pp.150–161. https://doi.org/10.1016/S0034-4257(03)00096-8

Urban, M., Schellenberg, K., Morgenthal, T., Dubois, C., Hirner, A., Gessner, U., Mogonong, B., Zhang, Z., Baade, J., Collett, A. and Schmullius, C. (2021). Using Sentinel-1 and Sentinel-2 Time Series for Slangbos Mapping in the Free State Province, South Africa. *Remote Sensing*, [online] 13(17), p.3342. https://doi.org/10.3390/rs13173342.

Vilà, M., Gassó, N., Thuiller, W., & Pino, J. (2012). Potential distribution range of invasive plant species in Spain. *NeoBiota*, *12*, 25–40. https://doi.org/10.3897/neobiota.12.2341

Wepener, J.P. (2007). The control of Stoebe vulgans encroachment in the Hartbeesfontein area of the North West Province. *North-West University: Potchefstroom, South Africa*.

http://hdl.handle.net/10394/2044
Whittaker, R.H., Levin, S.A. and Root, R.B. (1973). Niche, habitat, and ecotope. *The American Naturalist*, *107*(955), pp.321-338. https://doi.org/10.1086/282837
Worku, G., Teferi, E., Bantider, A. and Dile, Y.T. (2019). Observed changes in extremes of daily rainfall and temperature in Jemma Sub-Basin, Upper Blue Nile Basin, Ethiopia. *Theoretical and Applied Climatology*, *135*(3), pp.839-854. https://doi.org/10.1007/s00704-018-2412-x
Xu, H., Zhang, F., Li, W., Shi, J., Johnson, B.A. and Tan, M.L. (2024). Spatial-temporal pattern of change in production-living-ecological space of Nanchong City from 2000 to 2020 and underlying factors. *Environmental Monitoring and Assessment*, 196(2), p.94. https://doi.org/10.1007/s10661-023-12249-8
Yan, H., Feng, L., Zhao, Y., Feng, L., Wu, D., & Zhu, C. (2019). Prediction of the spatial distribution of Alternanthera philoxeroides in China based on ArcGIS and MaxEnt. *Global Ecology and Conservation*, *21*, e00856. https://doi.org/10.1016/j.gecco.2019.e00856
Yang, X., Crews, K., Frazier, A.E. and Kedron, P. (2020). Appropriate spatial scale for potential woody cover observation in Texas savanna. *Landscape Ecology*, *35*(1), pp.101-112. https://doi.org/10.1007/s10980-019-00933-5
Zhao, R.F.; Wang, J.F.; Li, L.H.; Zhang, L.H.; Lu, H.T.; Jiang, X.Y.; Chen, X.D.; Han, Z.Y.; Cairang, D.Z.; Wang, H. (2024). Evaluation of alpine wetland ecological degradation based on alpine wetland degradation index: A case study in the first meander of the Yellow River. Ecol. Indic. https://doi.org/10.1016/j.ecolind.2023.111414